New Folder Name LIGO Conceptual Design Handbook 3 Document

DRAFT

FOR INTERNAL USE ONLY

LIGO Interferometer Conceptual Design Handbook

Version 2.0

Authors: LIGO Science Team

October 23, 1992

LIGO-T920001-02-D

Contents

Chapter 1
Introduction

The ICD Handbook lays out the conceptual design for initial LIGO interferometers, as determined by scientific requirements and technical goals. The design is described in terms of subsystems; associated with each subsystem is a set of requirements, specifications, interfaces and tests for qualification. The following topics are not included here: operations scenario, data analysis, subsequent interferometers, work breakdown, schedules, and cost.

The handbook is intended as a reference document for all scientists and engineers working on LIGO.

1.1 Dimensions and Properties of Initial LIGO Interferometers

The key dimensions and physical properties of the initial LIGO interferometers are listed in Table 1.1. The details of the vacuum systems are covered in the 89 Proposal [1]; we list here the dimensions most closely connected to the interferometers.

1.2 Performance Requirements

The initial LIGO interferometers should be sensitive in the frequency band from approximately 30 Hz to approximately 10 kHz. Sensitivity is specified by equivalent displacement noise of interferometer test masses as a function of frequency (displacement amplitude spectral density $\tilde{x}$, units of $\mathrm{m}/\sqrt{\mathrm{Hz}}$), or by strain noise, which is defined as displacement noise divided by interferometer arm length: $\tilde{h}(f) = \tilde{x}(f)/L$. Figure 1.1 shows the expected sensitivity of initial interferometers, and the dominant noise contributors: seismic noise, suspension thermal noise, and shot noise at low, intermediate, and high frequencies, respectively. For comparison with a gravitational signal, it also shows the "most

INTERFEROMETER PHYSICAL PROPERTIES		
PARAMETER	**VALUE**	**NOTES**
Site 1 Arm Length	L =2 km (half-length) L =4 km (full-length)	Multiple interferometers in common vacuum pipe
Site 2 Arm Length	L =4 km	Full-length only
Test Mass Mirrors		
Material	Fused Silica	Test Mass/Mirrors are monolithic. Precise dimensions TBD.
Diameter	≈25 cm	
Thickness	≈10 cm	
Curvatures		
Input Mirrors	Flat	
End Mirrors	R_c = 6 km (full-length) R_c = 3 km (half-length)	
Laser Wavelength	λ = 514.5 nm	

Table 1.1: Key Dimensions and Physical Properties.

optimistic'' neutron inspiral strength for a detection rate of 3 events per year. Appendix A shows how detection rates for inspiraling neutron stars (the most concretely predictable expected source) depends on the dominant noise sources. The design philosophy is to trade off, where possible, the different noise sources to maximize the detection rate. This approach has resulted in a design with the expected maximum sensitivity, as shown in Figure 1.1, near 150 Hz.

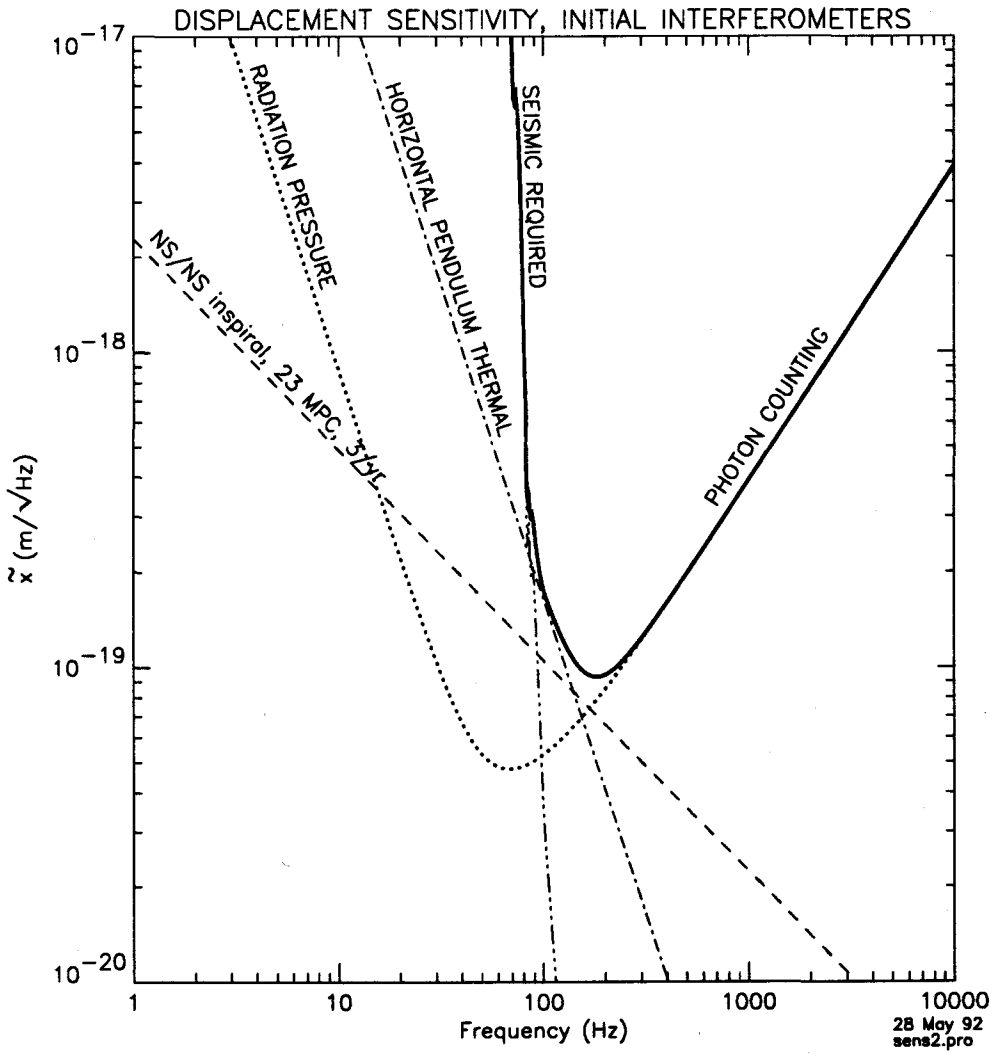

Figure 1.1: Expected displacement sensitivity of initial full-length (L = 4 km) LIGO interferometers (plotted with bold line), and contribution from the most significant noise sources. The *NS/NS inspiral* signal level was derived from Figure 10 of *Science* [3], by shifting that curve down by a factor of 11 to account for orientation and statistical corrections, and converting to displacement units by $\tilde{x} = h_c L/\sqrt{f}$. *RADIATION PRESSURE* and *PHOTON COUNTING* noise are the two types of shot noise discussed in Section 1.2.1 (Curve 2 of Figure 1.2 is plotted here); *SEISMIC REQUIRED* is the seismic noise described in Section 1.2.2; *HORIZONTAL THERMAL* noise is discussed in Section 1.2.3. Displacement noise levels are expected to be the same for half-length (L =2 km) interferometers, except photon counting (which is expected to be smaller) and radiation pressure (expected to be larger). The half-length and full-length interferometers will have the same power and storage times.

1.2.1 Shot Noise

Idealized Interferometer

The displacement sensitivity shot noise limit from photon counting at the main photodetector output of all initial LIGO interferometer configurations under consideration has the following frequency dependence:

$$\tilde{x}(f) = \tilde{x}_o\left(1 + [f/f_k]^2\right)^{1/2} \tag{1.1}$$

where f_k, the cavity knee frequency, is related to the arm cavity storage time by $\tau_e = 2L/c\mathcal{L}$ and to the mirror losses by $2\pi f_k = c\mathcal{L}/4L$; $\mathcal{L}$ is the total of transmission, absorption, and scattering losses for both mirrors making up an arm cavity of length L.

For a non-recycled interferometer,

$$\tilde{x}_o = \frac{\lambda}{2\pi}\mathcal{L}\frac{\sqrt{2}}{8\sqrt{\dot{N}}} \tag{1.2}$$

and the effective photon flux $\dot{N}$ is related to the efficiency-corrected power P incident on the beamsplitter by $P = \dot{N}hc/\lambda$. This result[1] applies to an idealized recombined system ([15], [2]) and also to an optimized modulated system where transmission is the dominant loss [13].

To extend this result to power recycling, $\dot{N}$ is replaced by $B_{\rm rec}\dot{N}$ (see Table 1.2 for definition of $B_{\rm rec}$).

Interferometers with Recycling and Modulation

The recycled interferometer shot noise has been calculated for a range of parameters in the externally modulated initial LIGO configuration under investigation at MIT [16]. The precise value of the shot noise depends on the arrangement of pick-offs and on the distribution of losses. As illustration, two optimized cases, identified as "Interferometer 1 with no contrast defect," and "Interferometer 3" (which includes an additional output cavity to pass "ω_3" sidebands), give shot noise levels corresponding to $1.22x_0$ and $0.83x_0$, respectively[2].

[1] Used to prepare the shot noise curves in the 89 Proposal [1], and in *Science* [3]. It is lower than the shot noise in the non-recombined configuration of the 40 m interferometer (in the low loss, low modulation limit) by $\sqrt{6}$.

[2] The "Interferometer 1" configuration with an assumed contrast defect of 1×10^{-3} has noise corresponding to $1.41x_0$ (not shown in figure 1.2).

A calculation of the unbalanced Michelson configuration under study at Caltech [10] gives a result very close to the "Interferometer 1, no contrast defect" result: $\sqrt{3/2}x_0 = 1.22x_0$.

Parameters and Comparison

The parameters relevant to shot noise and their values are listed in Table 1.2. Figure 1.2 shows the displacement sensitivity corresponding to different shot noise calculations.

Symbol	Description	Value	Notes
λ	Laser wavelength	514 nm	
L	Arm Length	4 km	
m	Cavity mirror mass	10.8 kg	Sets radiation pressure noise.
T_1	Input mirror power transmission	3%	T_1 assumed to be dominant loss. Noise insensitive to T_1 for $f > f_k$.
T_R	Transmission of recycling mirror	3.3%	
P_{circ}	Circulating power in arm cavities	3.9 kW	
I_{cav}	Intensity on cavity mirrors	540 W/cm^2 180 W/cm^2	@ input coupler @ output coupler
P_{BS}	Circulating power at beam splitter	60 W	
I_{BS}	Intensity on beam splitter	8.3 W/cm^2	
f_k	Knee frequency	90 Hz	$2\pi f_k = cT_1/4L$.
ηP	Power incident on recycling mirror	2 W	Corrected for inefficiencies. May be achieved, e.g., with 3 W out of input mode cleaner, 75% efficiency of remaining optics, and 90% photodetector quantum efficiency.
B_{rec}	Recycling factor	30	Defined as power buildup in arm cavities, compared to non-recycled cavities. Scattering and absorption losses alone allow larger B_{rec}; assumed limited by recombined beam contrast defect.

Table 1.2. Parameters that affect shot noise (high frequency) and radiation pressure noise (low frequency).

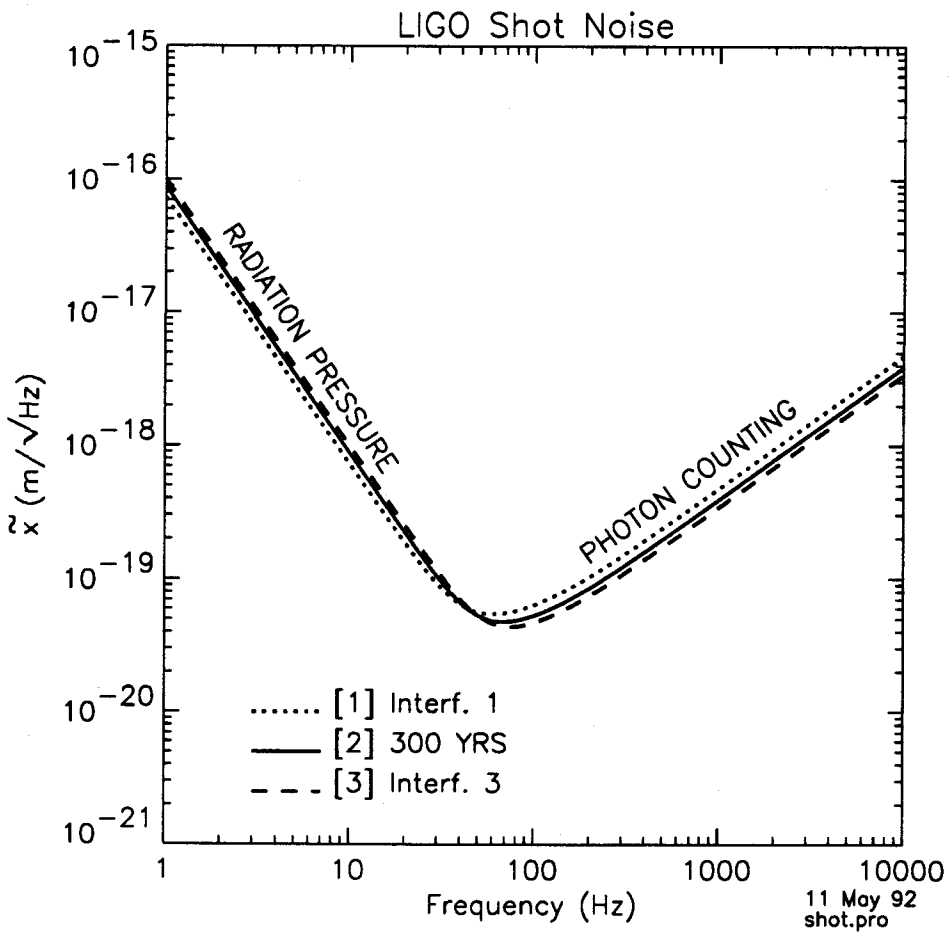

Figure 1.2. Shot noise calculation of photon counting and radiation pressure fluctuations for a system described by the parameters in Table 1.2. The radiation pressure lines intersect the photon-counting curves and the standard quantum limit (not shown; see [15]) at 41, 50, and 57 Hz, for curves 1, 2, and 3, respectively. Curves 1 and 3 are from [16], "Interferometer 1 with no contrast defect," and "Interferometer 3," respectively. Curve 2 corresponds to Equations 1.1 and 1.2. A preliminary calculation of the unbalanced Michelson variant [10] matches curve 1.

1.2.2 Seismic Noise

Linearly Coupled Seismic Noise

Ground motion excites an interferometer test mass after being filtered by an isolation stack and a wire suspension. To first order, the interferometer responds only to motions of the test masses along the beam line. Because of the curvature of the earth and misalignments, local vertical is not perpendicular to the beam line for all the test masses; consequently there is some contribution to interferometer noise from vertical motion of the test masses. Below approximately 90 Hz, the interferometer sensitivity is expected to be limited by direct linear coupling of seismic motion (assuming a 4 layer stack with viton as the elastomer). The strain noise due to seismic excitation is the product of 3 components:

1. Ambient ground motion
2. Stack isolation
3. Suspension isolation

Figure 1.3 shows the seismic noise requirement and goal for the initial LIGO interferometers. The "SEISMIC GOAL" curve shows the level of isolation that we believe can be achieved by the initial interferometer; it is significantly better than the "SEISMIC REQUIREMENT" level.

Components of Linearly Coupled Seismic Noise

The ground motion is determined by the specific sites that have been selected. Table 1.3 specifies a "standard spectrum" which is used as our basis for seismic noise estimates. It is a fit to measurements taken at locations throughout the United States. Ambient ground motion is fairly isotropic; consequently, the standard spectrum is the same in both the vertical and horizontal directions. Excitations due to tilts and rotations of the earth are assumed to be second order effects.

The ground noise is filtered through an isolation stack that functions as a passive low pass filter. The number of poles of the filter is twice the number of stack layers.

Since the test mass suspension wires are only 25 cm long, a connection between the top of the stack and the top of the test mass suspension is necessary for the test mass to reach the beam line (see Figure 1.4). This connector will be a rigid structure in the initial LIGO and will be termed the "vertical connecting

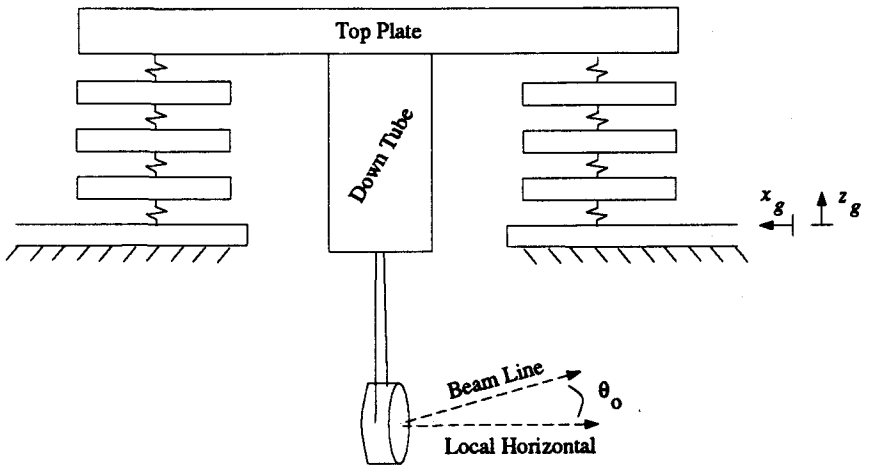

Figure 1.4: Possible Configuration of LIGO Test Mass Isolation System.

tube". The vertical connecting tube has a moment arm at least as long as the height of the stack; consequently, it will directly couple tilts from the top of the stack to horizontal motion of the test mass.

Additional filtering comes from a pendulum suspension connected to the base of the vertical connecting tube. The pendulum suspension acts as a seismic four pole low pass filter in both the horizontal and vertical directions.

The displacement noise spectrum $\tilde{x}$ due to seismic motion is a function of the stack and suspension parameters (see Table 1.4) and the horizontal and vertical ground motion x_g and z_g, respectively.

$$\tilde{x}(f) = \frac{2}{f^2}\left[\left[f_h^2 H_{xx} + f_h^2 R H_{\theta x} + \theta_o f_v^2 H_{zx}\right]^2 x_g^2 + \left[f_h^2 H_{zx} + \theta_o f_v^2 H_{zz}\right]^2 z_g^2\right]^{\frac{1}{2}} \tag{1.3}$$

Nonlinear Coupling

Larger low frequency (below approximately 15 Hz) motions of the test mass can also affect interferometer output in three ways:

1. Motions along the beam axis that perturb optical resonance.
2. Angular motions that change the pointing of the test mass.
3. Motions transverse to the beam line causing noise via irregularities in mirror scattering.

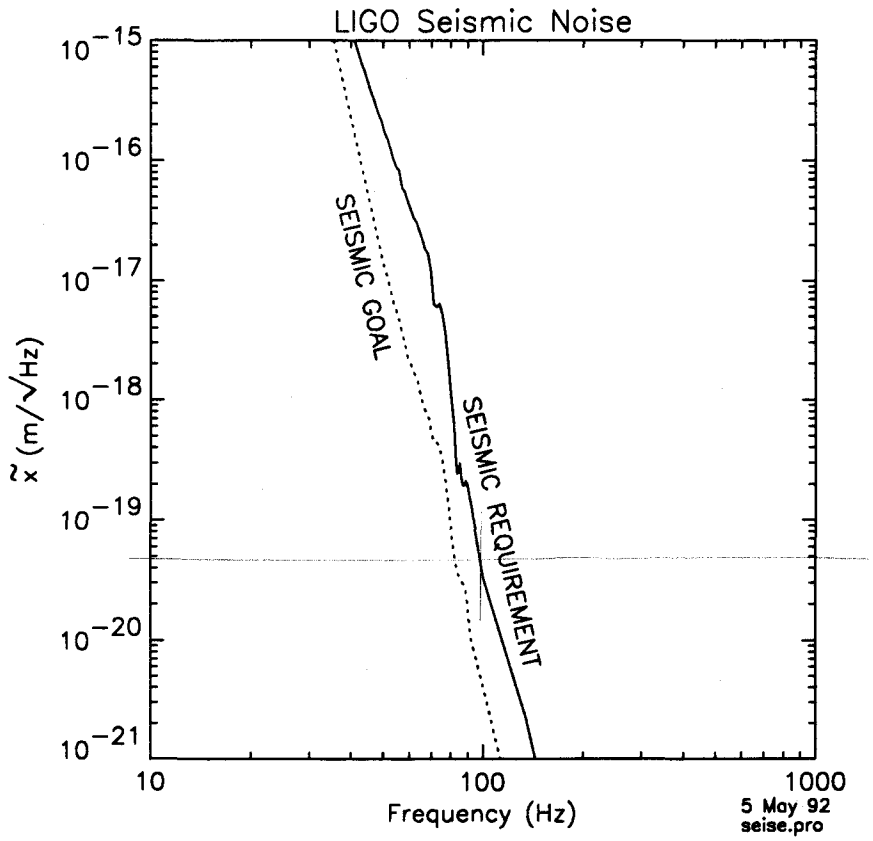

Figure 1.3: Requirement and Goal for Seismic Noise Contribution to Strain Spectrum.

FREQUENCY	AMPLITUDE
.1-1 Hz	$\frac{10^{-9}}{f^3}\frac{m}{\sqrt{Hz}}$
1-10 Hz	$10^{-9}\frac{m}{\sqrt{Hz}}$
10-10000 Hz	$\frac{10^{-7}}{f^2}\frac{m}{\sqrt{Hz}}$

Table 1.3: Adopted Standard for Ground Motion at LIGO Sites

Symbol	Description	Value
f_h	Pendulum horizontal resonance	1 hz
f_v	Pendulum vertical resonance	15 hz
θ_o	Angle of interferometer beam relative to local horizontal	.5 mrad
R	Height of vertical connecting tube	90 cm
H_{zz}, H_{xz}	Coupling coefficients from vertical ground motion to vertical and horizonal top plate motion, respectively.	see [14]
H_{zx}, H_{xx}	Coupling coefficients from horizontal ground motion to vertical and horizontal top plate motion, respectively.	see [14]
$H_{\theta x}$	Coupling coefficent from horizontal ground motion to the pitch angle of the top plate.	see [14]

Table 1.4: Stack and Suspension Parameters Used to Calculate Seismic Displacement Noise.

These higher order couplings, especially motions transverse to the beam line, are difficult to quantify.

The requirement on low frequency motion along the beam axis is stated in terms of rms motion of the test mass and is as follows: the total differential motion of a test mass must be less than 6×10^{-11}m. This level of motion keeps the effective storage time of each arm cavity matched to 1% [12]. The requirement on the total angular motion of a test mass is dictated by the contrast. In order to maintain a contrast in the interferometer of $C > \left(1 - 1 \times 10^{-3}\right)$, the rms alignment of the LIGO cavities must be held to within 2×10^{-7}rad (see [12] for a more detailed discussion). Servo loops are required to reach these low levels of RMS motion since the net horizontal single mirror motion is estimated to be 3.5×10^{-7} m RMS and the net angular single mirror motion around the vertical axis is estimated to be 3.5×10^{-7} rad RMS [12]. There is as yet no specification for the maximum allowed test mass motions transverse or vertical to the beam line; consequently, it has not been determined whether transverse or vertical damping of the test mass is necessary.

The requirement on motion of auxiliary optics is not as stringent, but has not yet been specified.

1.2.3 Thermal Noise

Each mode of a mechanical system has $\frac{1}{2}k_BT$ of energy (k_B the Boltzmann constant, T the absolute temperature). Equating this energy with the average kinetic energy of an oscillator $mv^2/2 = m\omega_0^2x^2/2$ of the mode of (effective) mass m and resonant frequency ω_0 allows us to calculate the mean-square displacement $x_{\text{thermal RMS}} = \sqrt{k_bT/m\omega_0^2}$. This motion will be distributed in frequency according to the losses in the oscillator.

If the losses are due to viscous damping (force F proportional to the velocity, $F = -\alpha v$; e.g., a dashpot), then the displacement noise spectrum is

$$\tilde{x}(f) = \left[\frac{4k_BT\alpha}{\left(k - m(2\pi f)^2\right)^2 + \alpha^2(2\pi f)^2}\right]^{\frac{1}{2}} \frac{\text{m}}{\sqrt{\text{hz}}} \tag{1.4}$$

The restoring force (gravity for the horizontal mode of the pendulum, or the material stiffness for a mirror internal mode) is represented by $F = -kx$, where the unsubscripted k is the usual Hooke's spring constant ($\omega_0 = \sqrt{k/m}$). The quality factor Q is related to the damping coefficient by $Q = m\omega_0/\alpha$.

Although experimental data confirmation is needed, we believe that the most likely loss mechanism for most of the critical LIGO systems is an internal damping which gives a force proportional to the displacement $F = -\phi(f)x$. This may be parameterized by a complex force constant: $F = -k(1 + i\phi(f))x$, giving a spectrum of displacement:

$$\tilde{x}(f) = \left[\frac{4k_BTk\phi(f)}{2\pi f\left(\left[k - m(2\pi f)^2\right]^2 + k^2\phi(f)^2\right)}\right]^{\frac{1}{2}} \frac{\text{m}}{\sqrt{\text{hz}}} \tag{1.5}$$

Equations 1.4 and 1.5 are plotted in Figure 1.5 with ϕ equal to a constant (the most likely case). The two curves differ because of the extra f in the denominator of the internally damped curve, giving a slope of $f^{-1/2}$ below the resonance and a slope of $f^{-5/2}$ above the resonance. We specify ϕ in terms of an equivalent internal damping on resonance $Q_{id} = 1/\phi$ to compare with viscous damping. See [11], page 243 for more detail and discussion.

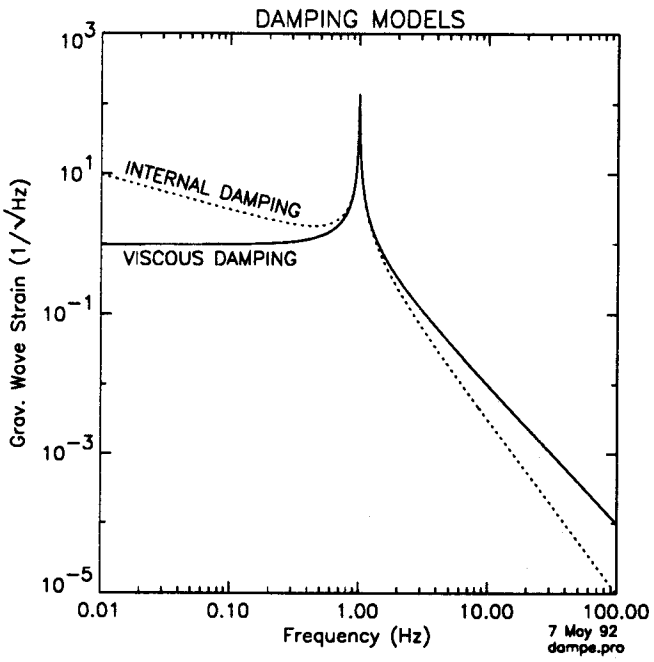

Figure 1.5: Resonance Curves for Viscously Damped System and Internally Damped System.

Estimates of the thermal noise based on material and design parameters are adopted as the requirements. To deal with the lack of experimental data, we choose the more conservative model for loss when determining the performance requirement.

Thermal Noise in Pendulum Suspensions

In the pendulum suspension, we are concerned with the thermal noise above resonance; the pendulum has a horizontal mode at roughly 1 Hz. The number, shape, and kind of suspension fibers and the terminating impedance of the suspension wires at the pendulum support point determine the thermal noise level .

For the calculations here, we assume a single tungsten wire loop which forms the suspension for a cylindrical test mass. The suspension wires are assumed to be stressed at about half their breaking strength. The parameters used for the model of the suspension are summarized in Table 1.5. This results in a horizontal pendulum frequency of $f_h = 1$ Hz, and a vertical pendulum frequency of $f_v = 15$ Hz.

PROPERTY DESCRIPTION	VALUE
Tungsten Wire Density	$15 \times 10^3 \frac{kg}{m^3}$
Wire Radius	1×10^{-4}m
Pendulum Length	.25m
Young's Modulus	$3.5 \times 10^{11} \frac{N}{m^2}$
Mirror Mass	10.8kg
Temperature	300°K

Table 1.5: Parameters Used In Suspension Model.

We choose a conservative model for the damping mechanism, and an optimistic Q for the interferometer requirement: viscous damping as described by Equation 1.4 and a $Q = 10^7$. Measurements of the internal loss of suspension wire materials are not in contradiction with this Q value, although there is no direct measurement to support it. The resulting displacement noise is shown in Figure 1.6 and falls as $1/f^2$ above 1 hertz.

The vertical oscillation of the pendulum also exhibits thermal noise. As above, the loss mechanism is not well understood, and so the more conservative viscous damping is assumed. The Q_v is expected to be lower than for the horizontal pendulum because the oscillator energy is stored in the wire, not in the earth's gravitational field. The pendulum vertical Q is taken to be $Q_v = 10^4$. For the motion to appear on the optic axis, a cross coupling from vertical motion of the pendulum wires to horizontal motion of the mirror is needed. It is sure to be at least .5 mrads (due to the curvature of the earth over 4 km), but may be greater due to lack of levelness of the site or imperfections in the suspension; we use 5×10^{-4}. The displacement noise is shown in Figure 1.6 and falls as $1/f^2$ above 15 hertz.

The transverse suspension wire mode ('violin string' resonance) thermal noise will not limit the noise floor of the interferometer, but will present a series of narrow spectral peaks spaced at (approximate) multiples of the fundamental frequency which with likely suspension properties will be about 650 Hz. We take a simple model where the excitation of the wire modes is calculated using either Equation 1.4 or 1.5, then the impedance mismatch going from the wire to the mass is used to calculate the resulting motion of the test mass. We use here a separately determined Q for the transverse modes. We ignore any contribution from the longitudinal modes of the suspension.

The $Q_{\text{string}_{id}}$ for the fundamental string mode on resonance is taken to be 3×10^5. An internal damping model is assumed. The expected noise is indicated in Figure 1.6 as "WIRE". The peak value of the fundamental string mode at 650 Hz is about $10^{-20} \frac{\text{m}}{\sqrt{\text{Hz}}}$.

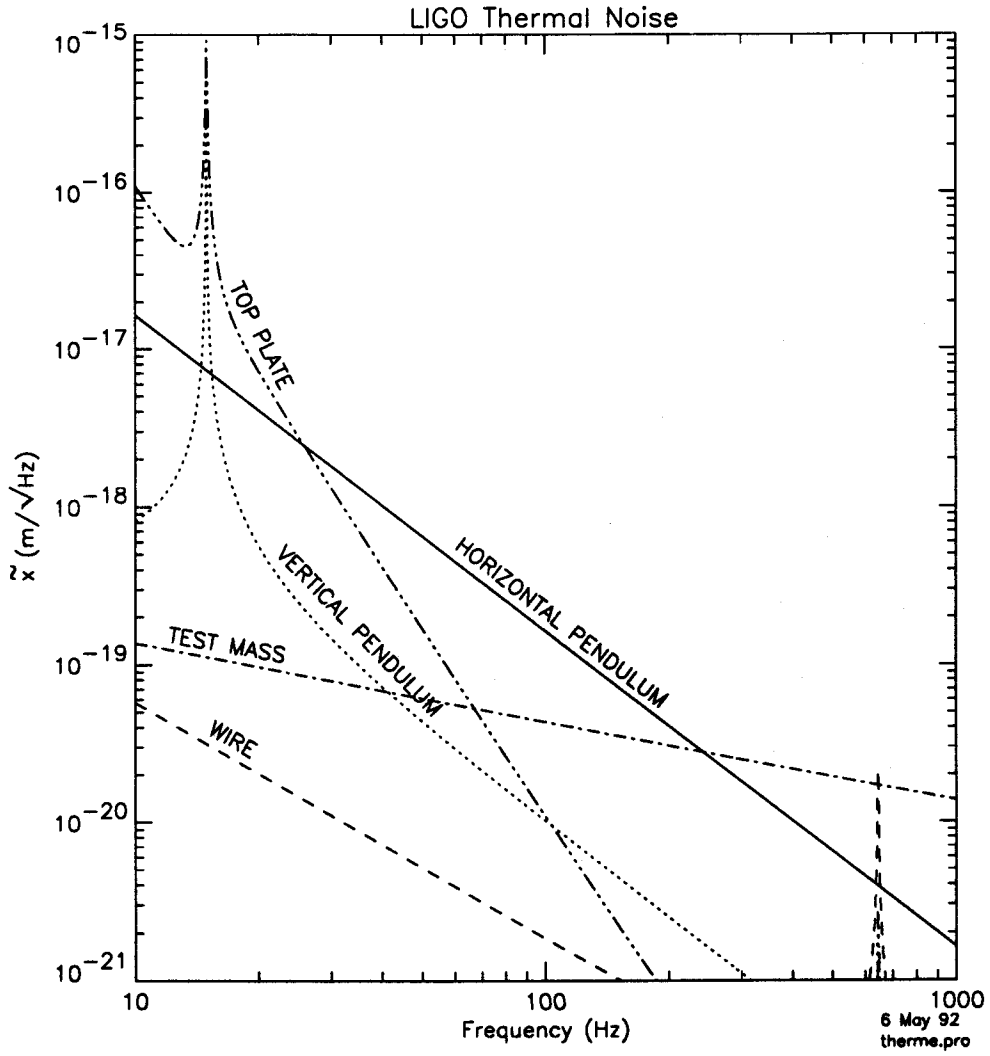

Figure 1.6: Thermal Noise Contribution to Strain Spectrum.

Thermal Noise in the Seismic Isolation Stack

The seismic isolation stack is a resonant system that exhibits thermal noise. We analyze only the oscillatory system consisting of the top plate mass and the springs/dampers upon which it sits, and disregard the remainder of the stack due to its second order contribution.

The horizontal oscillation (direct excitation of the suspension point) and the horizontal rotational oscillation (coupled through the vertical connecting tube) between the stack top plate and the pendulum suspension point) are considered. The parameters for the model are taken from the LIGO prototype stack, Jan '92. In this design, a deliberate low Q is chosen for the resonances (to reduce the level of motion due to seismic excitation on the resonance). The loss as a function of frequency for the Viton elastomer used as the spring and damper in the stack has been measured to be roughly constant with frequency. To be on the conservative side, though, a viscous damper model with a $Q_{\text{stack}} = 5.0$ is used. The other parameters are m=100 kg, $\omega_{o_h} = 2\pi \times 2$ Hz, $\omega_{o_v} = 2\pi \times 6$ Hz, coupling vertical to horizontal (vertical connecting tube length)/(stack top plate diameter)= 1.0. Note that the level at a given frequency grows as $\omega_o^{1/2}$. This excitation is filtered by the suspension pendulum, which is assumed to have a transfer function of $\left(\omega_{o_{\text{pend}}}/\omega\right)^2$, $\omega_{o_{\text{pend}}} = 2\pi \times 1$ Hz; this leads to the displacement noise shown in Figure 1.6. The curve is labelled "TOP PLATE" and falls as f^{-4}.

Thermal Noise in Mirror Substrates

The mirror substrate resonant frequencies lie above the gravity wave band, so we are interested in the thermal noise below the resonant frequency. The first few piston and annular resonant modes of the test mass contribute significantly, as does the + mode (two radial nodal lines at 90^o) which is derated based on the symmetry of the beam on the + mode.

As in the case of the pendulum, the correct model for the thermal noise has not been determined (although there is an experiment underway [9]). The more conservative estimate comes from an assumption of internal damping (ϕ=constant). A large high-quality substrate has shown measured Qs of 2×10^5 to 4.5×10^5 for several modes [4]. Further experiments with attachments and means of suspension are needed (and are underway in Orsay and Caltech).

The internal damping is taken to be that due to a Q on resonance of $Q_{\text{mirror}_{\text{id}}} = 10^6$. The mode frequencies used are 9.5×10^4 Hz (+ mode, with

a derating factor for the + mode of 10^{-1}), 1.4×10^4 Hz for a flexure mode with a circular nodal line (the dominant contribution), and a series of longitudinal modes starting at 2.8×10^4 Hz. Figure 1.6 shows an estimate of the thermally induced displacement noise and is labeled "Test Mass". It was calculated using the quadratic sum of the substrate modes. The curve has a slope of $1/\sqrt{f}$ at frequencies below the first substrate mode.

1.2.4 Other Noise Sources

Residual Gas Noise

1.3 Design Overview

The proposed basic design is a combination of the design outlined in the 1989 LIGO proposal [1] and subsequent designs and demonstrations. As shown in Figure 1.7, the overall Gravitational Wave Interferometer can be divided up into four major systems: an Input Optics System, an Interferometer System, a Data Acquisition and Interferometer Operations (DAIO System), and an Environmental Monitoring System.

The Input Optics System generates and conditions the laser light for the interferometer system. The prestabilized laser is a modified single Argon ion laser capable of an output power of 5 W (single mode). This laser is both frequency and amplitude stabilized by active servo loops. The mode cleaner subsystem will use a combination of one or more resonant Fabry–Perot cavities in transmission to stabilize further the frequency, amplitude, position and direction of the light. This will be followed by a set of injection optics which will mode match, point and otherwise condition the beam prior to passing it to the interferometer system.

The Interferometer System is the central part of the Gravitational Wave Interferometer. The optical interferometer senses the motion of test masses at the ends of the interferometer. The interferometer will operate in a Michelson configuration, with Fabry–Perot cavities in each arm to increase the sensitivity. The Fabry–Perot cavity in each arm of the interferometer will have a storage time of roughly 2 ms. Broadband recycling in the Michelson interferometer will be used to increase the circulating light power by a factor of 30. The differential phase shift induced by gravitational strain may be detected by interfering the light from the Michelson beamsplitter's antisymmetric output port with a phase modulated reference beam, derived from the illuminating light, in an external Mach–Zehnder interferometer arrangement, or by intentionally creating a small imbalance in the Michelson interferometer which will cause a small modulation of the light at the dark port. Pendulum suspensions will be used for the optical components, with active damping and steering from local sensors and drivers. A passive isolation stack employing unencapsulated elastomer springs will be used as the first stage of seismic isolation. An automated optical alignment system will be intrinsic to the design of the interferometer and will provide signals to the suspension and control system to control the alignment of the interferometer.

The DAIO System will monitor and control adjustable parameters of the system, as well as record all data from the Interferometer, Input Optics, and Environmental Monitoring System necessary to analyze the output for gravitational wave signals. The breakdown of the DCS into subsystems is not yet determined.

The Environmental Monitoring System consists of the instrumentation that monitors environmental factors that influence the interferometer's performance. Such factors include background magnetic field, seismic background at the vertex and end stations, cosmic ray background, temperature, etc. The Monitoring system interfaces with the DAIO system where the data is used for vetoing possible astronomical events that correlate with significant environmental events. The breakdown of the Environmental Monitoring System has not yet been determined.

1.3.1 Handbook Organization

The structure of the handbook follows closely the functional blocks pictured in Figure 1.7. Each of the major subsystems is described in its own chapter. Each subsystem is then broken into its own set of constituent blocks. The subsystem blocks were chosen to maximize the testability of each of the blocks. There is overlap in the design of many of the functional blocks since some of the components that appear in one block also appear in other blocks. For example, there is a seismic isolation subsystem (which is a part of the Interferometer System) and there is seismic isolation as a part of the mode cleaner. Rather than attempting to eliminate all such cases, we have adopted the working assumption that any overlap should be handled by cross-reference. In this example, the description of the mode cleaner seismic isolation would reference one of the standard designs of the seismic isolation subsystem, with any special requirements or modifications noted. Information that supplements the design effort can be included in the Appendix of the handbook or referenced to other documentation (such as the LIGO Working Papers).

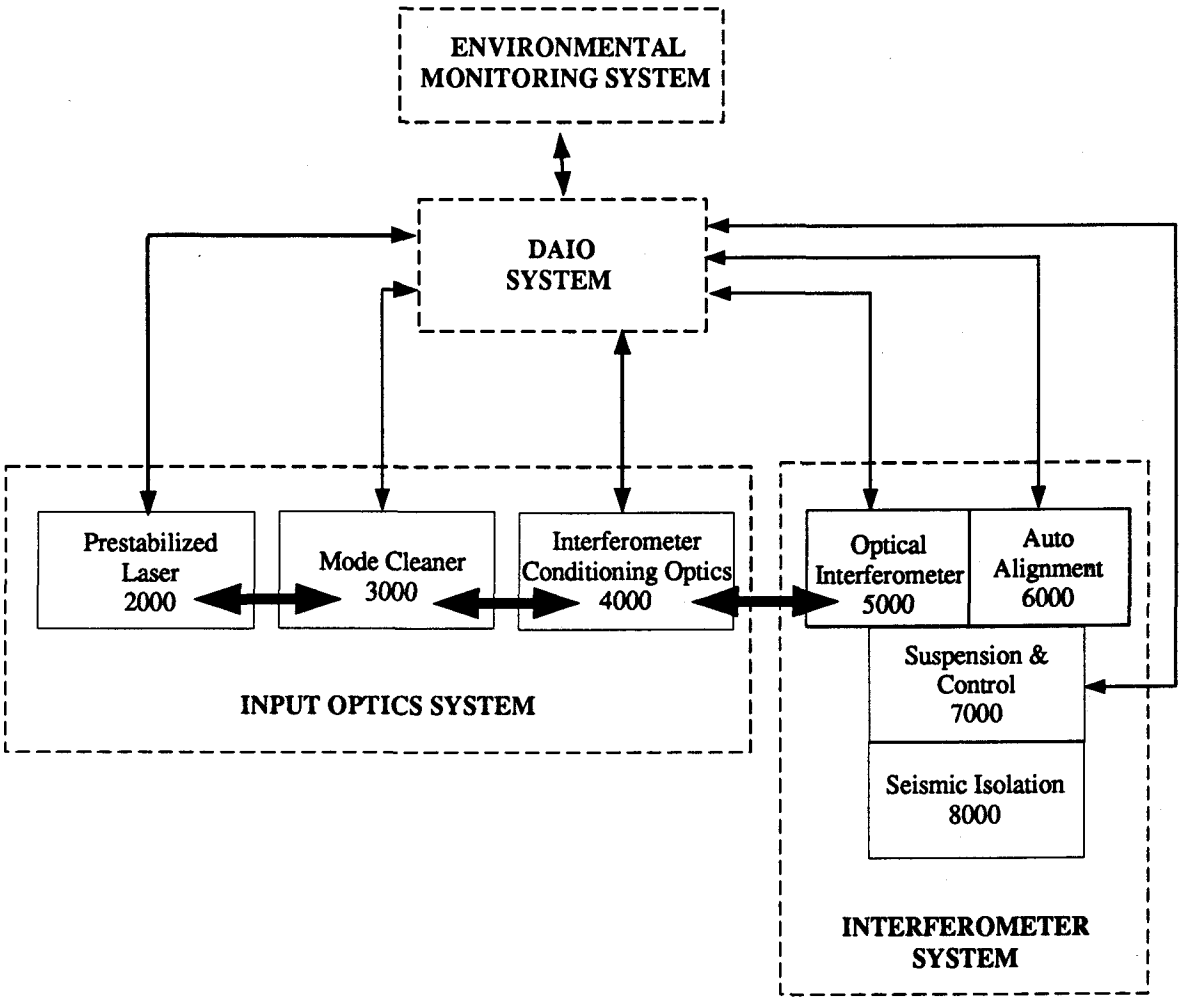

Figure 1.7: Functional Blocks of Gravity Wave Interferometer.

Chapter 2
ICD 2000 Prestabilized Laser

The function of a prestabilized laser subsystem is to provide an interferometer with light at a wavelength of 514.5 nm. It should operate at a sufficient power level, and provide adequate beam conditioning, so that the required interferometer sensitivity can be achieved.

There will be one prestabilized laser subsystem per interferometer; consequently, two subsystems at Site 1 and one subsystem at Site 2.

2.1 Functional Requirements

1. The prestabilized laser will deliver 3.5 W output power. This will ensure a minimum of 2 W at the recycling mirror.
2. The light delivered to the input optical chain will have its frequency stabilized down to 10^{-2} Hz/Hz$^{1/2}$, above 1 kHz, and down to a limit that is slowly increasing towards lower frequencies. This is shown explicitly in Figure 2.1. Frequency fluctuations at this level can be suppressed by frequency stabilization servo systems downstream, to a level compatible with LIGO sensitivity requirements.
3. The frequency of the prestabilized laser is meant to track the length of the mode cleaner. This will be achieved by feeding the error signal, derived at the mode cleaner, back to the laser, which will function as a voltage controlled oscillator (VCO). The two inputs for the tracking signal are called "slow VCO", and "fast VCO".
4. Relative optical power fluctuations will be kept down to 3×10^{-7} /Hz$^{1/2}$, above 1 kHz, and down to a limit that is slowly increasing towards lower frequencies (see Figure 2.2). At this point, this requirement is somewhat artificial, and is meant to improve upon the raw intensity noise of the laser currently used with the 40 m prototype.

5. Laser mode hopping will be eliminated, in order to ensure long term, stable operation of the interferometer.
6. The pointing stability and the mode purity of the beam will be no worse than for the laser currently used with the 40 m prototype
7. Requirement on uptime/maintenance: TBD. One spare laser head, complete with power supply and cooling unit, but not including mirrors, will be kept at each site. A complete set of optical components (list TBD) will also be kept at each site.

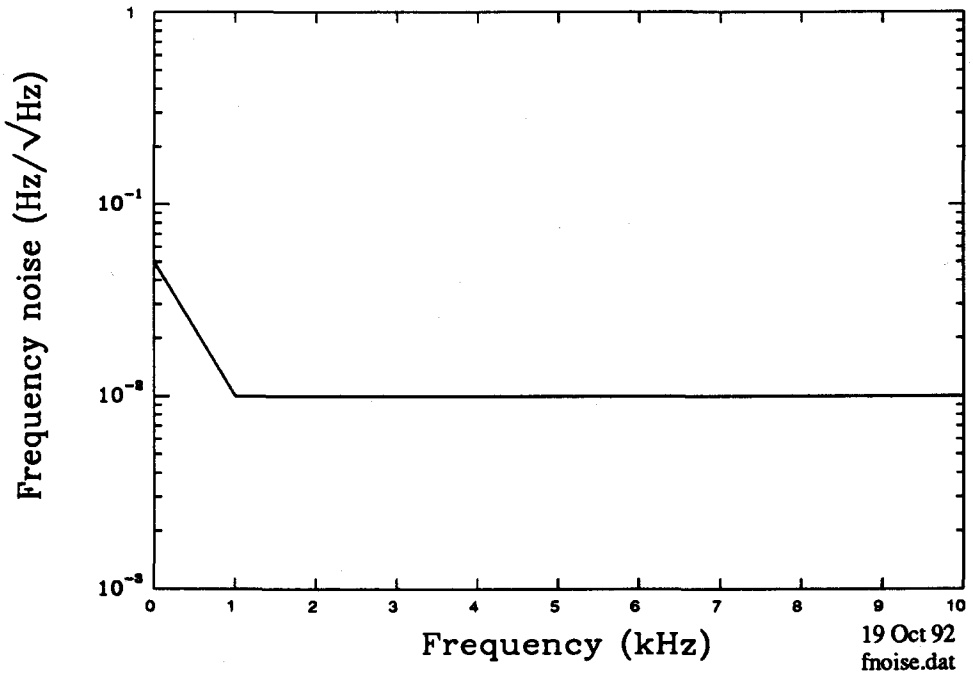

Figure 2.1: Frequency stability goal for the prestabilized Spectra Physics laser.

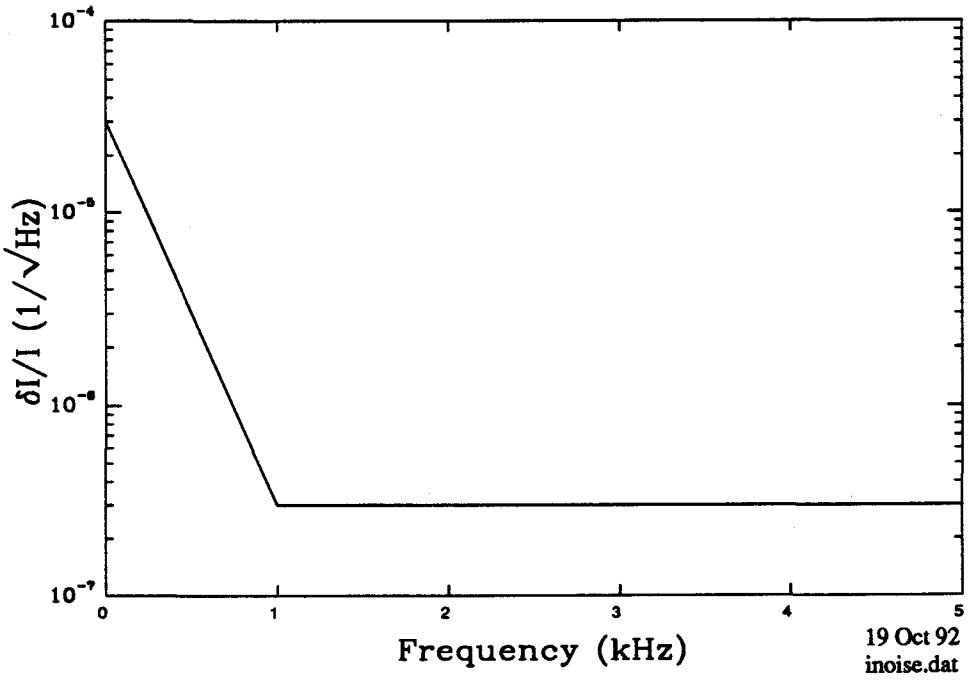

Figure 2.2: Power stability goal for the prestabilized Spectra Physics laser.

2.2 Block Diagram and Subsystem Description

The prestabilized laser subsystem consists of a modified commercial laser, the power stabilization, and the frequency stabilization (see Figure 2.3).

All components of the prestabilized laser subsystem are in air, except for the reference cavity (see Figure 2.5), which is suspended from a seismic isolation stack inside a small vacuum chamber.

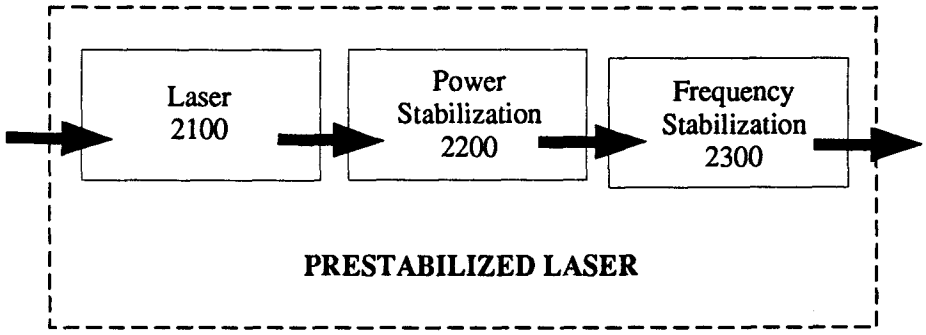

Figure 2.3: ICD2000 Prestabilized Laser Block Diagram

2.2.1 ICD 2100 Laser

The laser is a modified version of a 2040E Spectra-Physics large frame argon ion laser configured for 5 W single line output at 514.5 nm. The in-house modifications consist of separating the laser mirrors from the laser tube/cooling system, and providing the mirrors with piezo-electric transducers for frequency correction. Figure 2.4 shows schematically how the as-purchased Spectra Physics laser is modified. The mirrors are detached from the frame, PZT transducers are added to the mirrors, and the PZT-mirror assemblies are attached to sturdy mirror mounts. These mirror mounts are bolted to a superinvar optical breadboard in order to reduce changes in laser resonator length when the ambient temperature changes. The superinvar breadboard is isolated from the optical table by one layer of RTV springs. The laser head is also isolated from the optical table but with a 3 layer stack of lead and RTV springs. An external dry nitrogen purge is used instead of the factory provided purge.

An itemized layout of the optical and mechanical components, including part numbers and drawing numbers, can be found in [7]. The electronic circuit diagrams and transfer functions are documented in [5].

2.2.2 ICD 2200 Power Stabilization

The power stabilization subsystem consists of an acousto-optic modulator, photo detector, servo amplifier, and iris/beam dump. The layout of the power stabilization subsystem is shown in Figure 2.5. Drawings and part numbers for the optical and mechanical components are found in [7]. The electronic circuit diagrams and transfer functions are documented in [5].

2.2.3 ICD 2300 Frequency Stabilization

The frequency stabilization subsystem consists of the piezo-electric transducers supporting the laser mirrors (Figure 2.4), and the other elements inside the heavy-dashed block in Figure 2.5. Circuit diagrams and transfer functions of the electronics are documented in [5] while the drawings and part numbers for the mechanical and optical components are included in [7].

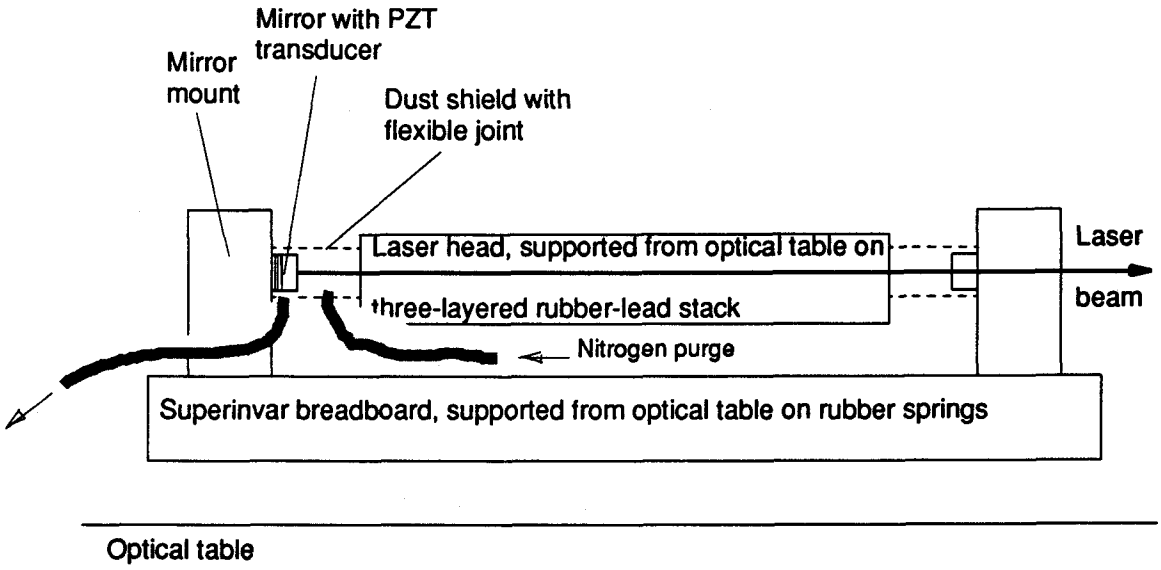

Figure 2.4: Modified Spectra Physics laser

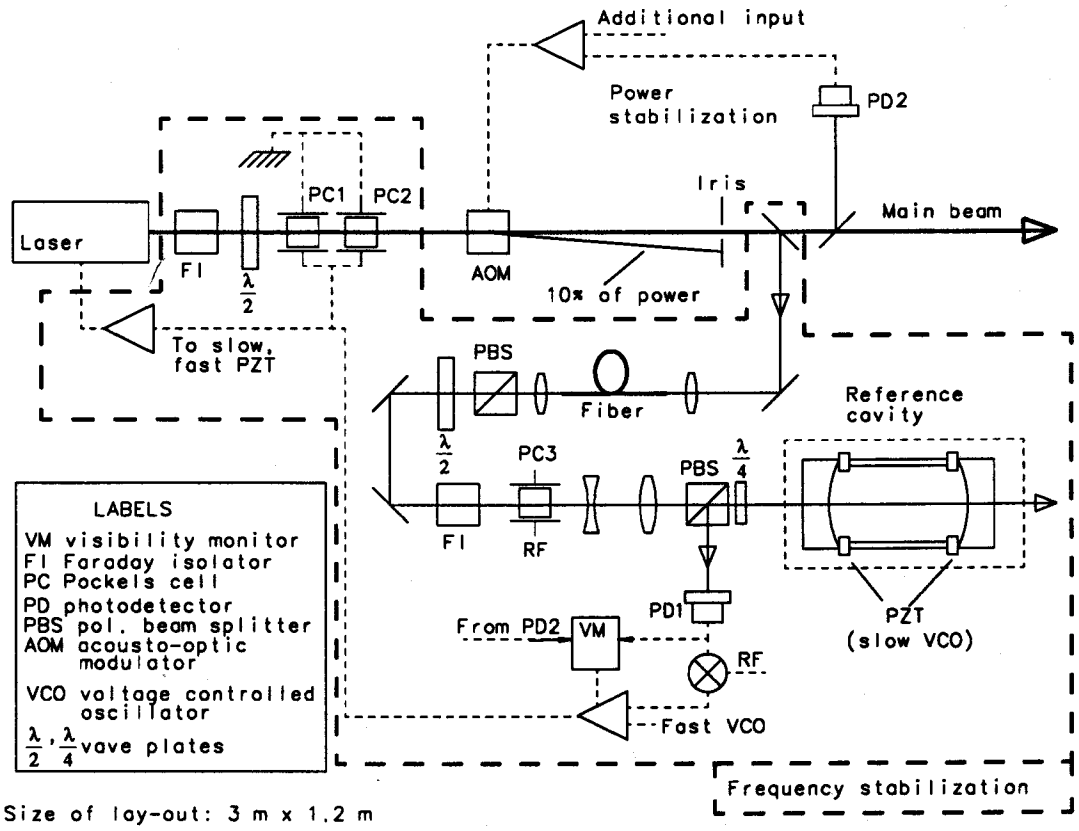

Figure 2.5: Prestabilized laser optical layout. The Frequency Stabilization components are in the heavy dashed box. The Power Stabilization components are in the upper right hand corner of the layout.

2.3 Methods for Testing Subsystem Blocks

The following acceptance tests should be performed, for each laser, prior to shipping to the LIGO sites, and after installation in LIGO.

2.3.1 Test Procedure for ICD 2100 Laser

Upon implementing the necessary modifications, and installation at the LIGO site, the laser will be tested as follows:

1. The modified laser will be tested for maximum power. At least 5 W of single frequency, single transverse mode green light should be measured

at the output, using a separate power meter. In the process, the internal power meter of the laser will be calibrated. Single frequency operation will be checked with an optical spectrum analyzer (preferably a 215 Coherent spectrum analyzer with 300 MHertz free spectral range). Single transverse mode operation will be checked by using the optical spectrum analyzer, and by visual examination of the beam, after expansion to a diameter of $\sim$10 inches, by using a lens.

2. The piezo-electric transducers will be driven over their full ranges, by using a 1 Hz triangle or sine wave of appropriate amplitude, in order to check, by using the optical spectrum analyzer, that the light can be tuned over the specified frequency range.
3. Upon installation at the LIGO site, the laser will be hooked up to the DAIO, and a remote control/monitoring test will be carried out.

2.3.2 Test Procedure for ICD 2200 Power Stabilization

This subsystem will be tested by measuring the power fluctuations with a separate photo detector that feeds an audio frequency spectrum analyzer, e.g. 3563 HP. The ratio between these fluctuations and the DC output of the sampling photodetector will be compared with the power stability goal of Figure 2.2.

2.3.3 Test Procedure for ICD 2300 Frequency Stabilization

This subsystem will be tested as follows:

1. After adjusting the gains at various points in the servo preamplifier, the signals at the monitor points will be inspected for signs of anomalous behavior (oscillation, out of range state), by use of an oscilloscope.
2. The demodulator output will be fed to an RF spectrum analyzer, and checked whether it is suppressed by the servo below the shot noise level, as defined by a flashlight test.
3. The residual frequency noise will be measured by using an analyzer cavity (a cavity dedicated for that purpose or possibly the mode cleaner). The demodulator signal from the reference cavity will be compared with a calibration signal, generated by impressing a low frequency (0–10 kHz) FM on the laser beam, by using a Pockels cell. The measured frequency noise will be compared with the goal defined by Figure 2.1.

2.4 Interfaces

2.4.1 Interfaces with Other Subsystems

- Optical interface: The laser is the source of the green light that is injected into the mode cleaner subsystem.
- Electronic interfaces:
    a. Inputs for signals from light-to-mode cleaner locking servo: slow and fast VCO
    b. Inputs for signals from light-to-interferometer locking servo: slow and fast VCO.
    c. Additional input to light intensity stabilization servo
    d. Digital interface with DAIO

2.4.2 Interfaces with the Environment

- Electrical interface with the mains
- Mechanical interface with the floor
- Acoustic interface with the surrounding air
- Thermal interface with the environment, via the laser resonator length and the reference cavity length

Requirements Placed on Environment by the Prestabilized Laser

The performance requirements for the prestabilized laser subsystem imply the following types of requirements on elements of the environment, interfaced with the laser:

1. Limits on air turbulence. TBD
2. Limits on acoustic noise. TBD
3. Limits on seismic noise. TBD
4. Electric power and cooling requirements. TBD
5. Limits on ambient temperature variation. TBD
6. Limits on power line disturbance and electromagnetic radiation caused by laser power supply. TBD

All the above limits will be compared with similar limits imposed by other LIGO subsystems. The more stringent limits will prevail.

2.5 Data and Control Signal Definition

The following table is a summary of the servo control signals needed to control a Prestabilized Laser subsystem. It also includes the requirements placed on each of the signals to ensure the subsystem is operating within the specifications stated in Section 2.1.

SIGNAL	ORIGIN	DESTIN-ATION	TYPE	BW	CENTER FREQ.	RANGE (Vpp)
RF mod. signal	RF oscillator	PC3	analog	0 Hz (sine wave)	9 MHz	20
RF ref. signal	RF oscillator	mixer	analog	0 Hz (sine wave)	9 MHz	9
DC PD current	PD1 front end	Visibility monitor	analog	0 Hz	DC	10
DC PD current	PD2	Visibility monitor	analog	0 Hz	DC	5
Bypass on/off	Visibility monitor	Servo amplfier	TTL	0 Hz	DC	5
AC PD current	PD1 front end	mixer	analog	600 kHz	9 MHz	2(?)
Primary error signal	mixer	Servo amplifier	analog	300 kHz	DC	0.2
Phase correction	Servo amplifier	PC1, PC2	analog	2 MHz	1 MHz	800
Fast PZT signal	Servo amplifier	Laser, Fast PZT mirror	analog	100 kHz	50 kHz	300
Slow PZT signal	Servo amplifier	Laser, Slow PZT mirror	analog	1 kHz	0.5 kHz	800
Fast VCO (EXT)	Mode cleaner, Interf (EXT)	Servo amplifier	analog	500 kHz	250 kHz	0.1
Slow VCO (EXT)	Mode cleaner, Interf. (EXT)	Ref. cavity PZT	analog	1 kHz	0.5 kHz	1

SIGNAL	ORIGIN	DESTIN-ATION	TYPE	BW	CENTER FREQ.	RANGE (Vpp)
Interf. noise	PD2	Interf. stabil. amplifier	analog	100 kHz	50 kHz	5
Interf. noise (EXT)	Additional sampler (EXT)	Interf. stabil. amplifier	analog	100 kHz	50 kHz	0.1
Interf. noise correction	Interf. stabil. amplifier	AOM	analog	100 kHx	50 kHz	1

Figure 2.6: Servo control signal definition and specifications. Listed signals are those which travel through cable from origin to destination. Signals labeled "EXT" originate from sources external to the prestabilized laser subsystem. Element abbreviations in Columns 2 and 3 (e.g. PD1, PD2, PC1, PC2, PC3, PZT, and AOM) refer to electro-optical components shown in Figure 2.5.

2.6 Developmental Status

A prestabilized laser, as described above, has been built and tested. All functional requirements have been met, except for the one corresponding to residual frequency noise, which was measured at a level 3–10 times higher than required. Also, a contamination source that could not yet be pinned down made the life-span of the reference cavity too short to be useful. The following steps are being taken to bring the system up to the required specifications:

1. The design of the reference cavity has been modified, to exclude epoxy adhesive
2. "Dirty" RTV rubber, used for the seismic isolation, will be replaced with cleaned RTV. This and the previous step are expected to reduce the contamination level substantially.
3. The new reference cavity will be tested, at first, without the PZT disks, in order to determine whether the disks may be the source of contamination.
4. It is hoped that eliminating the epoxy joints will reduce the residual frequency noise, which is suspected to be caused by 'glue noise'.
5. The length of the reference cavity will be increased from 34 cm to 50 cm, in order to make it easier to tune the laser to a reference cavity

resonance. If, as suspected, the residual frequency noise is due to local mirror displacement noise, this will also reduce the noise by one third.

3
ICD 3000 Mode Cleaner

Describe the function of the Mode Cleaner subsystem from a top level perspective.

3.1 Functional Requirements

3.2 Block Diagram and Subsystem Description

The Mode Cleaner subsystem can be divided up into the MC Conditioning Optics module, Modulation module, MC Cavity module, MC Suspension and Control module, and MC Seismic Isolation module.

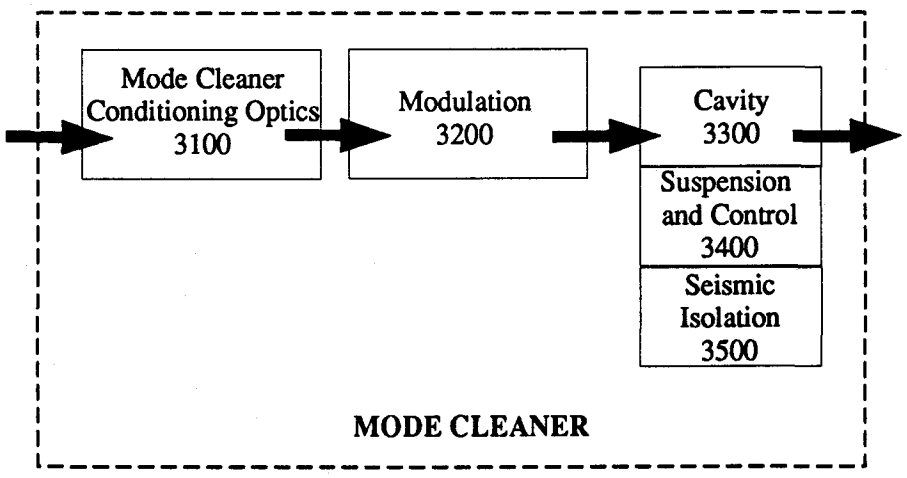

Figure 3.1: ICD3000 Mode Cleaner

3.2.1 ICD 3100 Mode Cleaner Conditioning Optics

3.2.2 ICD 3200 Mode Cleaner Modulation

3.2.3 ICD 3300 Mode Cleaner Cavity

3.2.4 ICD 3400 Mode Cleaner Suspension and Control

The design of a suspension and control module are described in Chapter 7. Things to be discussed here are those issues specific to the mode cleaner. Cross references to 7 should be used whenever possible

3.2.5 ICD 3500 Mode Cleaner Seismic Isolation

The details of a HAM seismic isolation are discussed in Chapter 8. Things to be discussed here are those issues specific only to the mode cleaner isolation. Cross references to 8 should be used whenever possible.

3.3 Methods for Testing Subsystem Blocks

3.4 Interfaces

3.5 Data and Control Signal Definition

SIGNAL	ORIGIN	DESTIN-ATION	TYPE	BW	CENTER FREQ.	RANGE (Vpp)
R/I/T	DCS			Very Low		

Table 3.1: Data and Control Signal Definition and Specifications.

3.6 Developmental Status

Chapter 4
ICD 4000 Interferometer Conditioning Optics

Describe the function of the Interferometer Conditioning Optics Subsystem from a top level perspective.

4.1 Functional Requirements

4.2 Block Diagram and Subsystem Definition

The Interferometer Conditioning Optics subsystem can be divided up into the Conditioning Optics Module, the Suspension and Control Module and the Seismic Isolation Module.

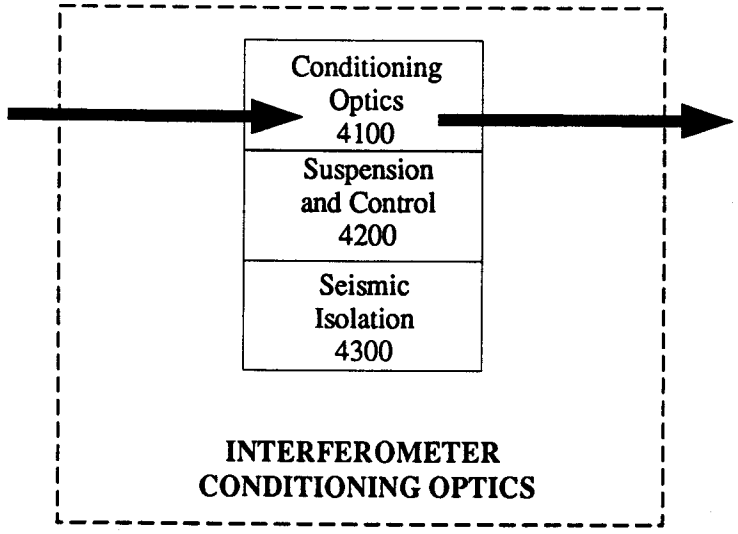

Figure 4.1: ICD4000 Interferometer Conditioning Optics

4.2.1 ICD 4100 Conditioning Optics

4.2.2 ICD 4200 Conditioning Optics Suspension and Control

The design of a suspension and control module are described in Chapter 7. Things to be discussed here are those issues specific to the conditioning optics. Cross references to 7 should be used whenever possible

4.2.3 ICD 4300 Conditioning Optics Seismic Isolation

The details of a HAM seismic isolation are discussed in Chapter 8. Things to be discussed here are those issues specific only to the conditioning optics. Cross references to 8 should be used whenever possible.

4.3 Methods for Testing Subsystem Blocks

4.4 Interfaces

4.5 Data and Control Signal Definition

SIGNAL	ORIGIN	DESTIN-ATION	TYPE	BW	CENTER FREQ.	RANGE (Vpp)
R/I/T	DCS			Very Low		

Table 4.1: Data and Control Signal Definition and Specifications.

4.6 Developmental Status

Chapter 5
ICD 5000 Optical Interferometer

Chapter 6
ICD 6000 Auto Alignment

Chapter 7
ICD 7000 Suspension and Control

Chapter 8
ICD 8000 Seismic Isolation

The function of the seismic isolation is to attenuate the ambient ground noise at frequencies in the gravity wave band.

There are 4 types of seismic isolation designs corresponding to the 4 chamber types: type 1 and 2 test mass chambers (TMC1 and TMC2), diagonal chambers, and horizontal-axis module (HAM) chambers. The dimensions of the stack and the type of elastomer used depend on the chamber type. The input optics, output optics, and recycling mirror are mounted on the HAM stacks, the test mass optics are mounted on the TMC1 and TMC2 stacks, and the beam splitter optics are mounted on the diagonal stacks.

The TMC1 chambers are placed at locations in LIGO where executing routine maintenance on the test mass in the plane along the beam aperture would disturb the operation of the other interferometers. To keep from disturbing the other interferometers, the TMC1 includes a mechanism for lifting the test mass above the 4 foot beam aperture through a horizontal air lock unit (see 89 Proposal [1]).

TMC2 seismic isolation is used at all test mass locations in LIGO where maintenance of the test mass in a plane along the beam aperture does *not* interfere with the operation of the other interferometers, thus there is no need for a lift mechanism. The number of chambers necessary at each site in the initial LIGO configuration are listed in Table 8.1.

	SITE 1	SITE 2
# of Interferometers	2	1
# of TMC1 Chambers	4	0
# of TMC2 Chambers	4	4
# of Diagonal Chambers	2	1
# of HAM Chambers	$\approx$ 12	$\approx$ 6

- lifts

Figure 8.1: Number of Chambers at Sites 1 and 2.

8.1 Functional Requirements

Figure 1.3 shows the maximum permitted seismic noise contribution to the strain spectrum. This requirement can be reached if the transfer functions of each stack (TMC1, TMC2, and Diagonal Chamber) are equal to or below the measured prototype stack transfer functions shown in [6]. The isolation requirement for the HAM stack is not as demanding, but has net yet been specified. The amount of isolation required by a HAM stack will be driven by the most sensitive component suspended from the stack; at present this is the recycling mirror.

The electrical cabling that is routed up the side of each of the stacks must be mounted in such a way that it does not degrade the isolation performance of the stack.

The thermal and mechanical properties of the elastomer springs of the stack induce a drift in the angular and translational position of the stack over hour and month time scales, respectively. It is necessary to control the stack translations and rotations over at least month time scales (probably not hour time scales). This is discussed in more detail in Section 8.2.1.

The seismic isolation stack should be equipped with "motion stops" to protect the stack from moving too far from its equilibrium position in the event of an earthquake or other unexpected large disturbance. Provisions should also be designed into the stack that will send an error message to the operator, in the event that the "motion stops" are degrading the seismic isolation.

8.2 Subsystem Description and Block Diagram

The natural division of the ICD 8000 Seismic Isolation into subsystems is to divide it into blocks consisting of each of the stack types. This division is shown explicitly in Figure 8.2.

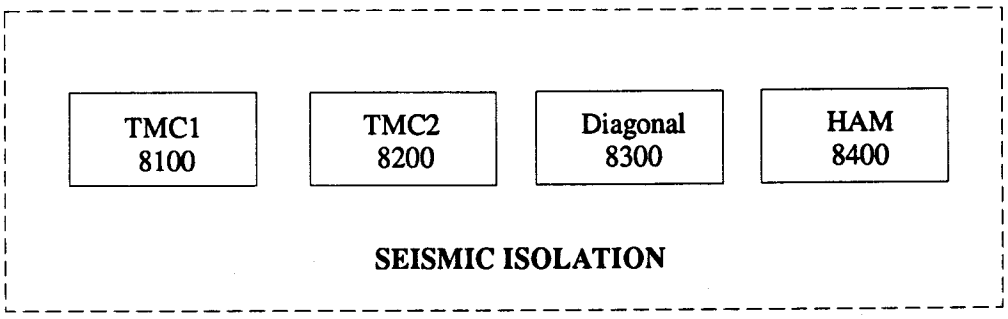

Figure 8.2: ICD8000 Seismic Isolation Block Diagram

8.2.1 ICD 8100 Test Mass Chamber 1 Seismic Isolation

The TMC1 seismic isolation assembly is made up of a stack, a support structure, and a drift compensation mechanism (see Figures 8.3 and 8.4). The stack provides the seismic isolation. The support structure provides a stiff structural interface to the out-of-vacuum support points. The drift compensation is an out-of-vacuum motorized system that compensates for drift in the stack due to the settling of the elastomer springs.

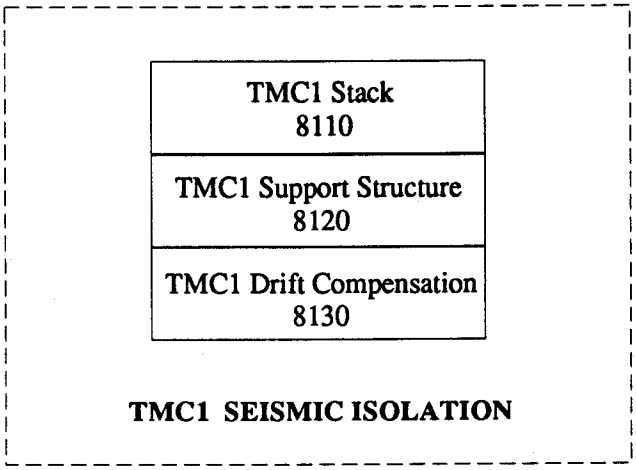

Figure 8.3: ICD8100 TMC1 Seismic Isolation Block Diagram

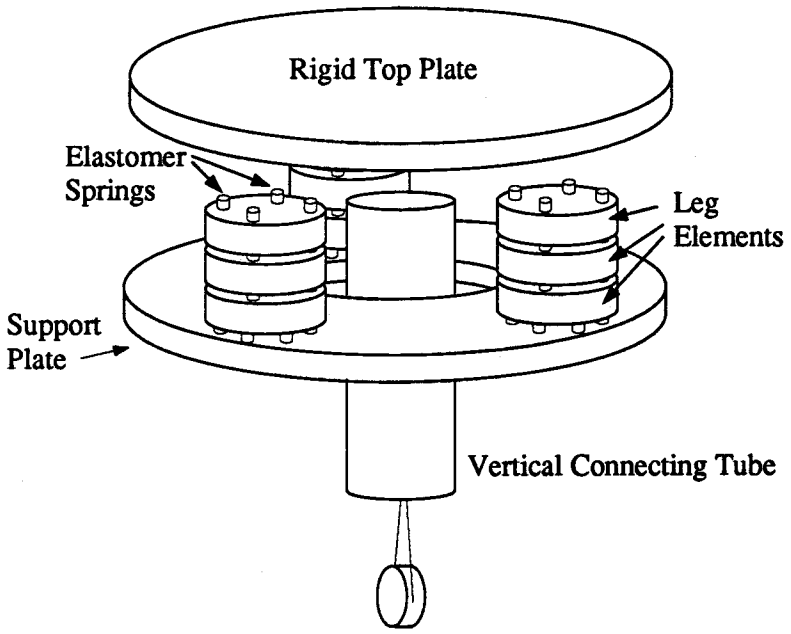

Figure 8.4: Example isolation assembly for TMC1. For correct scaling on the stack dimensions see Table 8.2.

ICD 8110 TMC1 Isolation Stack

The stack will be made up of 4 layers. Three legs will support an aluminum plate welded (or possibly bolted) to an aluminum vertical connecting tube. The plate plus connecting tube functions as the fourth layer of the stack. The vertical connecting tube provides a rigid interface between the top of the stack and a set of "hanging component suspension modules" defined in Chapter 5. Each of the legs will be made up of 3 identical elements. These elements are metal discs with recessed holes for the placement of the elastomer springs. The elastomer type assumed for the TMC1 chamber stacks is Viton.[3]

The requirement for the lowest allowed internal resonant frequency for each of the leg elements is calculated in [14]: $f_o > 400$ Hz. The lowest internal resonant frequency of each of the leg elements in one leg must vary by a minimum of 10%.[4]

[3] Viton is assumed to be the chosen elastomer since it is the closest to being vacuum qualified. If RTV can be vacuum qualified, the stack will probably be designed with 1 layer of Viton and 3 layers of RTV. The three layers of RTV are necessary to get better isolation while the Viton will be used to reduce the Q of the stack and to possibly damp the support plate.

[4] The exception to this rule is if the fundamental frequency of all of the leg elements is greater than 800 Hz. For this case, all of the leg elements can have identical internal resonances.

Requirements for the lowest internal resonant frequency of the top plate/vertical connecting tube are also calculated in [14]. The lowest internal resonant frequency of the top plate/connecting tube for a 4 layer Viton stack is $f_o > 310$ Hz. The assumptions used to calculate the frequency specifications are listed in [14]. The frequency specifications will change if RTV is vacuum qualified for use in LIGO. The specifications may also change when the site seismic surveys are available; in particular, stack resonances should not overlap with large resonances in the spectrum of ground motion. Table 8.2 shows the critical parameters needed for specifying the stack design.

The routing of the electrical cables to the top plate is a critical part of the isolation design. Cables in a TMC1 will run up a leg of the stack and be rigidly connected to each element of the leg. A half loop of wire will be used between each rigid connection. A complication arises at the interface between the last leg element and the top plate. The TMC1 has a mechanism that lifts the test mass well above the stack. The wires need to be long enough to accommodate raising the top plate 1.5 meters above the top leg element, but they cannot touch the leg elements or chamber walls when the top plate is resting on its legs.

ICD 8120 TMC1 Support Structure

The support structure holds the entire load of the stack and test mass. The support structure is made up of a stainless steel frame support (see drawing #1101018) with a stainless steel "support plate" (Figure 8.4) or a set of plates bolted on the frame. The lowest frequency of the support structure with a xxx pound load is specified to be 25 Hz. The assumptions used to calculate this frequency specifications are discussed in [14].

The support plate cannot be solid due to the presence of the vertical connecting tube; it will either have to be a ring or a set of 3 or 4 smaller plates welded to the support beams.

ICD 8130 TMC1 Drift Compensation

The drift compensation system corrects for drift in the top plate angular and translational position, resulting primarily from elastomer sag or temperature-correlated variations in elastomer dimensions.

The range and precision requirements are listed in Table 8.1. The compensators will be motorized for automatic control, unless it is determined that adjustments will be made less frequently than twice per year.

Adjustment	Range	Precision
Top plate height	+/- 7 mm	xxx mm
Top plate tilt (2 orthogonal angles)	xxx deg	xxx deg
Top plate rotation	xxx deg	xxx deg

Table 8.1: Range and Precision Requirements of Drift Compensation.

8.2.2 ICD 8200 Test Mass Chamber 2 Seismic Isolation

The TMC2 seismic isolation is identical to the TMC1 seismic isolation except in the way that the electrical cabling is routed up the stack. Since there is no lift mechanism, the top plate and the top leg element of the stack are never separated, consequently the cabling is simplified.

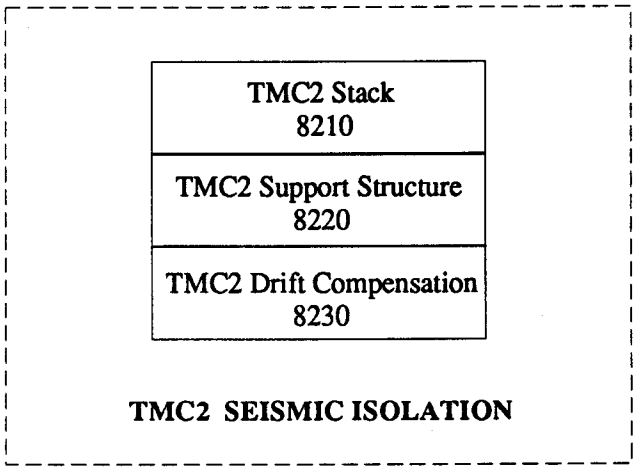

Figure 8.5: ICD8200 TMC2 Seismic Isolation Block Diagram

ICD 8210 TMC2 Isolation Stack

The ICD 8210 is identical to the ICD 8110 except in the way that the electrical cabling is handled. The cabling that runs to the top of a TMC2 stack will be rigidly connected to each element of one of the legs. A half loop of cable will be used between each rigid connection. The cable connection between the last leg element

and the top plate is the same as the connection between leg elements since the top plate is permanently positioned on top of the stack.

ICD 8220 TMC2 Support Structure

The ICD 8220 is identical to the ICD 8120 TMC1 Support Structure.

ICD 8230 TMC2 Drift Compensation

The ICD 8230 is identical to the ICD 8130 Drift Compensation system.

8.2.3 ICD 8300 Diagonal Chamber Seismic Isolation

The diagonal chamber seismic isolation is identical to the TMC2 isolation except for one feature; the base plate of the vertical connecting tube has a larger diameter. The larger diameter is necessary for accommodating more suspended components.

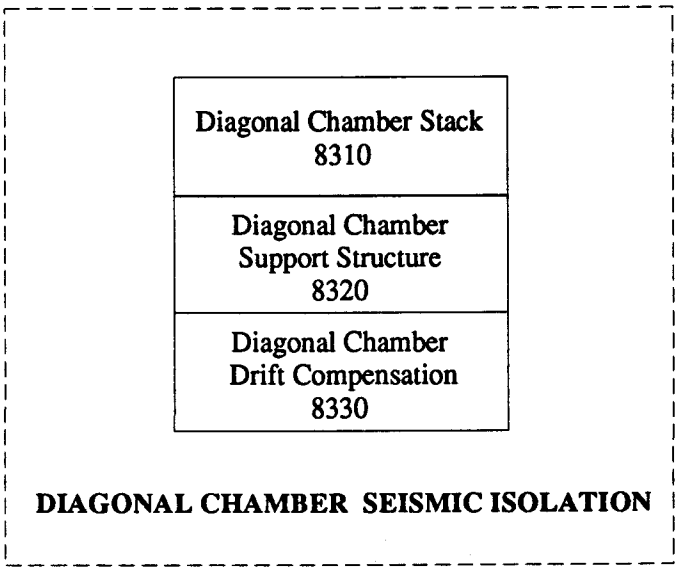

Figure 8.6: ICD8300 Diagonal Chamber Seismic Isolation Block Diagram

ICD 8310 Diagonal Chamber Stack

A number of elements of the ICD 8310 system are identical to the ICD 8210. This includes the leg elements, the top plate, the elastomer type[5], and the routing of the electrical cables. The vertical connecting tube is also identical except that the base plate of the connecting tube is larger in diameter.

The diameter of the TMC1 vertical connecting tube does not provide an adequate amount of space for mounting the optics in the diagonal chamber. A base plate with a larger diameter is needed. This plate will be bolted onto the mouth of the vertical connecting tube after the stack has been assembled in the chamber. The larger diameter base plate is not an option for the TMC1 stack since the connecting tube has to be raised above through a 5 foot aperture. Drawings of the beam splitter stack and a concept for assembling the stack and its optics are discussed in [8].

ICD 8320 Diagonal Chamber Support Structure

The ICD 8320 is identical to the ICD 8220 TMC2 Support Structure.

ICD 8330 Diagonal Chamber Drift Compensation

The ICD 8330 is identical to the ICD 8230 TMC2 Drift Compensation System.

8.2.4 ICD 8400 HAM Seismic Isolation

The HAM seismic isolation assembly is made up of a stack, a support structure, and a drift compensation mechanism. The Ham isolation differs from the rest of the isolation assemblies since it is smaller and the optics and suspension assemblies are mounted on top of the stack.

ICD 8410 Ham Stack

The HAM stack is made up of 4 layers. Three legs will support an aluminum plate that acts as the top layer of the stack. Each of the legs will be made up of 3 metal discs that have recessed holes for the placement of the elastomer springs. The elastomer type assumed for the HAM stacks will be chosen using the same

[5] In the event that the RTV is vacuum qualified, the elastomer types used for the stack will probably be 2 layers of RTV on the top and 2 layers of viton on the bottom. The 2 layers of viton would be used to keep the Q around 5, in order to minimize any spurious interferometer effects.

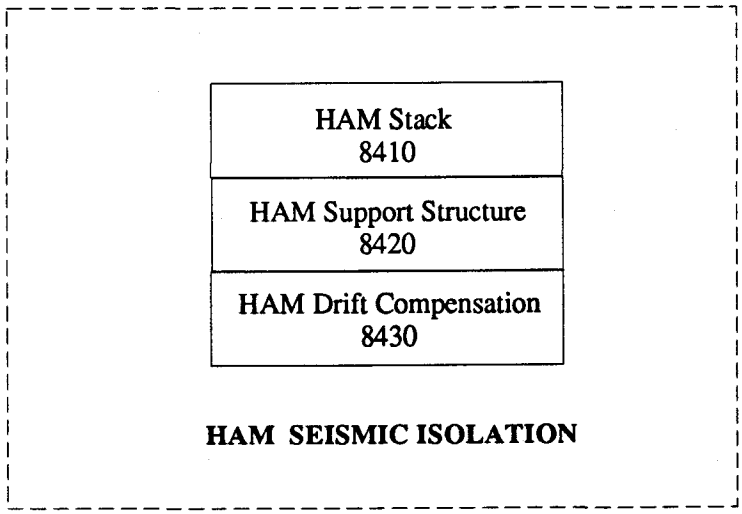

Figure 8.7: ICD 8400 HAM Seismic Isolation Block Diagram

rationale as for the diagonal chamber stacks. The frequency specifications for the metal parts of the stack were chosen using the same criteria as the frequency specifications for the TMC1 stack. Table 8.2 shows the critical parameters needed for specifying the stack design.

The wiring will be done in the same manner as that for the TMC2 stacks.

ICD 8420 HAM Support Structure

The support structure is made up of a stainless steel frame support (see drawing #1101941) with a stainless steel plate or a set of plates mounted on the frame for supporting the legs of the stack. The lowest frequency of the support structure with a (?) pound load is specified to be 25 Hz. This frequency specification was chosen similarly to the specifications for the TMC1 support structure.

The support structure plate will be a solid plate, a ring, or a set of 3 or 4 smaller plates welded to the support beams.

ICD 8430 HAM Drift Compensation

The ICD 8430 is identical to the ICD 8130 TMC1 Drift Compensation System.

	STACK TYPE		
	TMC1/TMC2	Diagonal	HAM
# of Layers	4	4	4
# of Legs	3 or 4	3 or 4	3 or 4
Leg Element Dimensions and Mass	diam = xxx in height = 5 in ? mass = xxx kg	diam = xxx in height = 5 in ? mass = xxx kg	diam = xxx in height = 5 in ? mass = xxx kg
Leg Element Material	stainless steel	stainless steel	stainless steel
Lowest Internal Resonance of Leg Element	400 Hz	400 Hz	400 Hz
Top Plate Dimensions and Mass	diam = 6 ft ? height = xxx in mass = xxx kg	diam = 6.5 ft ? height = xxx in mass = xxx kg	diam = 5 ft ? height = xxx in mass = xxx kg
Vertical Connecting Tube Dimensions	tube diam= 4.5 ft ? base plate diam=4.5ft height = xxx in wall thickness=xxx in	tube diam= 4.5 ft ? base plate diam=5.5ft height = xxx in wall thickness=xxx in	not applicable
Plate/Connecting Tube Material	aluminum	aluminum	aluminum
Lowest Internal Resonance of Plate/Connecting Tube	310 Hz	310 Hz	310 Hz
Elastomer Type	4 layers viton	4 layers viton	4 layers viton
# Springs per Layer	TBD	TBD	TBD
Location of Stack on Support Structure	symmetric about center	symmetric about center	symmetric about center
Load	TBD	TBD	TBD

Table 8.2: Critical Parameters for Phase 1 Stack Design.

8.3 Method for Testing Subsystem blocks

8.3.1 Qualification Testing

A qualification test qualifies a specific design to be used in LIGO. There will be tests done to qualify the stack seismic isolation, the drift compensation system, and the TMC1 lift mechanism.

There will be stack isolation tests done prior to the final qualification tests on smaller prototype stacks. These tests will, and are, being done in vacuum on a "scaled" version of one of the LIGO stack designs.

The optimal qualification test for the stacks would be a full-sized test in vacuum. If this is determined to be impractical, the stacks will be tested in air. The main difference between the TMC1, TMC2, and diagonal stacks is the elastomer type used, so tests can be done that are valid for all 3 stack types just by changing the elastomer in the test setup. A large test facility could conceivably be built in house. The test facility will be modeled after the test facility used for the Mark 2 stacks. The measurements will consist of ground noise excited transfer functions at frequencies below 20 Hz and shaker excited transfer functions at frequencies above 20 Hz. If the transfer functions measurements fulfill the requirements specified in Figure 1.3, the isolation assemblies will be qualified to go into LIGO.

8.3.2 Acceptance Testing

The acceptance tests must ensure that each individual stack used in LIGO is acceptable after installation. Once a stack has been installed, a power spectrum of the noise on the top of the stack will be taken. It should match up with a known power spectrum that is characteristic of the stack type and the ground noise expected at the site.

After each stack is assembled a test of the drift compensation system for each stack is also necessary. Each compensator will be tested to see that it meets the dynamic range requirements listed in Section 8.2.1.

After each TMC1 stack is assembled, the lift mechanism must also be tested to see if the top plate/vertical connecting tube can be raised to its maximum height for maintenance, and then replaced within the tolerances listed in Section 8.4.1.

8.4 Interfaces

The vertical connecting tubes of the ICD 8110, ICD 8210, and ICD 8310 interface with a number of "hanging component suspension modules" defined in Chapter 5. The top plate of the ICD 8110 also interfaces with a lift mechanism during the times when the stack optics need maintenance. The top plate of an ICD 8410 interfaces with a number of "hanging component suspension modules". The module types are defined in Chapters 3, 4, and 5.

The drift compensation system of the ICD 8130, ICD 8230, ICD 8330, and ICD 8430 each interface with a set of chamber bellows. The ICD 8130, ICD 8230, and ICD 8330 interface with cement pedestals outside of the vacuum envelope while the ICD 8430 interfaces with the floor outside of the vacuum envelope.

8.4.1 Requirements Placed on Interfaces by Seismic Isolation

A requirement is placed on the bellows at the interface between the vacuum chamber and the drift compensation system for each of the stacks. The bellows must be able to translate xxx mm in the horizontal, transverse, and vertical directions and they must also be able to sustain torques of xxx nt-meters with a duty cycle of xxx.

A requirement is also placed on the lift mechanism by the seismic isolation system. The top plate of the ICD 8110 needs to be replaced after maintenance on the optics with an accuracy of xxx mm.

8.5 Developmental Status

A prototype stack, not including a vertical connecting tube, has been built and tested [6]. The prototype meets the seismic requirement plotted in Figure 1.3. There will be at least one more iteration in the design process before we settle on the final LIGO stack designs. The final stack designs for ICD 8110, ICD 8210, ICD 8310, and ICD 8410 will be similar to the prototype but will be larger and flatter. The vertical connecting tube is still in the conceptual phase.

In writing this chapter it was necessary to assume an elastomer type (Viton was chosen) for the stacks so that calculations of different stack parameters were possible. Unfortunately choosing an elastomer at this time is premature since Viton, as well as RTV, has not been vacuum qualified yet. We are in the process of comparing the benefits of using Viton, RTV, or some combination of the two

in the LIGO stacks. Calculations [12] show that the RMS motion requirement listed in Section 1.2.2 is satisfied whether a Viton or an RTV stack is assumed. The effects of parasitic interferometers associated with optical component motion and upconversion due to motion transverse to the beam axis can be minimized or increased depending on the Q of the elastomer; although, it is very difficult to quantify the change in performance. The Viton has a $Q \approx 5$ and the RTV–615 has a $Q \approx 30$. Viton is a good choice for the diagonal and HAM chamber stacks since the parasitic interferometer effect increases with maximum velocity, and the low Q of Viton results in slower stack motion. The attenuation in the gravity wave band is most important for the test mass stacks, so we may choose to use the higher Q RTV which gives better isolation at $f \geq 30$Hz. As discussed in Chapter 7, damping of the test mass motion by magnetic feedback can compensate for the increased motion of an RTV stack. The damping could also be accomplished using passive resonant dampers. Research projects in progress will help determine whether the isolation stacks will be composed of all RTV, all Viton, or a combination.

The designs for the Support Structure ICD 8120, 8220, 8320, and 8420 have been partially completed. The support beams have been designed for each subsystem but the support plate and the interface between the support plate and the beams is still in the conceptual stage.

The design for the ICD 8130, 8230, and 8330, and 8430 Drift Compensation is still in the conceptual stage. The drift compensation system designed into Mark 2 will be our first experience with an out-of-vacuum drift compensation design. We expect to learn a number of lessons from this setup that will be applicable to the LIGO design.

Chapter 9
Data Acquisition and Interferometer Operations

Chapter 10
Environmental Monitoring System

Appendix A
Scaling of Coalescing Compact Binary Detection Rates with Initial Reciever Noise Parameters

Initial LIGO receiver strain sensitivity is expected to be limited by seismic noise, suspension thermal noise, and photocurrent shot noise at low, middle and high frequencies, respectively. A simple noise model parametrized by a *seismic cutoff frequency* f_s, an *effective pendulum quality factor* Q_e, and *effective laser power* P_e is used to compute the SNR, and thus the relative detection rate at a statistically significant threshold, for coalescing neutron star binary gravitational wave signals.

A.1 SNR and Detectable Event Rate

Following Thorne [15], the strain signal $u(t) \equiv s(t) + n(t)$ measured at the receiver output consists of gravitational wave strain signal s added to the receiver background noise n. The receiver noise n is presumed to be a stationary, random process, whose power spectral density

$$S_n(f) = \lim_{T\to\infty} \frac{1}{T} \left| \int_{-T}^{T} n(t) e^{-2\pi i ft} dt \right|^2 \tag{A.1}$$

is measured and known. For a given expected signal waveform *s(t)*, a Weiner optimal filter is constructed to filter the signal *u*. The squared output $U^2 = (S + N)^2$ of this filter is maximized when a true signal is present. The squared *signal-to-noise ratio* of an event is given by

$$\left(\frac{S}{N}\right)^2 = \int_0^\infty \frac{2|\tilde{s}(f)|^2}{S_n(f)} \tag{A.2}$$

where

$$\tilde{s}(f) \equiv \left[\int_{-\infty}^{\infty} s(t) e^{-2\pi i ft} dt \right] \tag{A.3}$$

is the Fourier transform of the event's waveform *s(t)*.

A threshold U^2_{min} is set which guarantees an acceptably small probability that $U^2 > U^2_{min}$ will occur randomly in the absence of a real signal (say, for example, less than one erroneous "detection" per 10 years). This threshold defines the minimum detectable strain signal size given the detector noise.

The signal waveform's amplitude is proportional to a factor $G(\theta,\phi,\psi,...)$ (define $\overline{G^2} \equiv 1$) which depends upon the relative orientation and polarization of the receiver and the source, which we will assume are randomly distributed, and is inversely proportional to the distance r between the detector and the source. We therefore write

$$s(t) = G(\theta, \phi, \psi, ...)s_o(t)\frac{r_0}{r} \tag{A.4}$$

where $s_0(t)$ is the expected signal from a "barely detectable" fiducial source which has typical polarization and relative orientation to the detector, and is placed at fiducial radius r_0 such that $U^2 = U^2_{min}$ at the time of the event.

Assuming that similar sources are randomly distributed in space, the *rate of detectable events* R is proportional to to the volume of the sphere of radius r_0, i.e.

$$R = ar_0^3 = \beta\left(\frac{S}{N}\right)^3 \tag{A.5}$$

where α and β are constants. We can therefore write

$$R = K\left[\int_0^\infty \frac{2|\tilde{s}(f)|^2}{S_n(f)}\,df\right]^{\frac{3}{2}} \tag{A.6}$$

where K is a constant.

A.2 Receiver Noise Model

The receiver noise n is presumed to be the quadrature sum of contributions from several independent stationary random processes, so that

$$n^2(t) = \sum_i n_i^2(t) \tag{A.7}$$

and

$$S_n(f) = \sum_i S_{n_i}(f). \tag{A.8}$$

Here we model three contributions, seismic, thermal and shot noise, considered most likely to dominate the spectrum for initial LIGO receivers.

A.2.1 Seismic Noise

The power spectral density of ground motion falls roughly as f^{-4} at frequencies above 10 Hz. For a four-layer stack, the anti-seismic isolation is expected to incorporate 4 complex pole pairs (around 10 Hz), and the pendulum suspension 1 complex pair (near 1 Hz), so the power spectral density of receiver seismic noise n_s is expected to fall as

$$S_{n_s}(f) \propto f^{-24} \tag{A.9}$$

in the frequency band of interest. This is sufficiently steep that, for plausible event spectra (Equation A.3), assuming a "brick wall" power spectrum

$$S_{n_s}(f) = \begin{cases} \infty & f \leq f_c \\ 0 & f > f_c \end{cases} \tag{A.10}$$

introduces negligible errors in Equation A.6 if we choose the *seismic cutoff frequency* f_c appropriately.

A.2.2 Thermal Noise

In the middle frequency band we expect suspension thermal noise to dominate other noise contributions in the initial receivers. We choose a viscous damping model for thermal noise in the pendulum suspension, partly for lack of a better model. As discussed in Section 1.2.3, this gives pendulum thermal noise contribution n_t with power spectral density

$$S_{n_t}(f) = 1.6 \times 10^{-37} \left(\frac{1\text{Hz}}{\text{f}}\right)^4 \left(\frac{10^7}{Q_e}\right) \tag{A.11}$$

for 10 kg test masses on 1 Hz suspensions. Here Q_e is the "effective" pendulum quality factor, physically meaningful only if the damping is strictly viscous, but otherwise simply a parameter.

A.2.3 Shot Noise

The photocurrent shot noise (Section 1.2.1) n_p is characterized by spectral density

$$S_{n_p}(f) = 1.7 \times 10^{-50} \left(\frac{f}{1\text{Hz}}\right)^2 \left(\frac{2\,\text{W}}{\text{P}_\text{e}}\right) \tag{A.12}$$

at frequencies well above the knee frequency f_k of the arm cavities. A recycling factor of 30 (????) has been assumed.

The model receiver noise spectrum is shown in Figure A.1 for an example choice of the three parameters f_c,Q_e and P_e.

A.3 Event Spectrum and Detection Rate

For coalescing compact binaries the strain signal increases in amplitude as it sweeps up in frequency; however, the signal spends relatively more time at lower frequencies, so the spectrum is weighted more heavily at the lower end. We presume the signal cuts off completely when the bodies collide, at a frequency of about 1 kHz for a neutron star pair [15]. The signal's Fourier transform has the form

$$|\tilde{s}(f)|^2 = \frac{A}{f^{\frac{7}{3}}} \tag{A.13}$$

up to this frequency, where A is a constant which depends on the masses of the objects, their orbit, their distance, and so on [see [15], Equation 44].

Equation A.6 then reads

$$R = K_0 \left[\int_0^{1\,\mathrm{kHz}} \frac{f^{-\frac{7}{3}}}{S_{n_s}(f) + S_{n_t} + S_{n_p}(f)} df \right]^{\frac{3}{2}} \tag{A.14}$$

where K_0 is a constant. For scaling convenience we will choose K_0 and A such that $R = 1$ for the the receiver parameters listed in Figure A.1.

Plots of Relative Event Rate versus f_c and Q_e (P_e fixed), and Relative Event Rate versus Q_e and P_e (f_c) fixed, are shown in Figures A.2 and A.3 respectively.

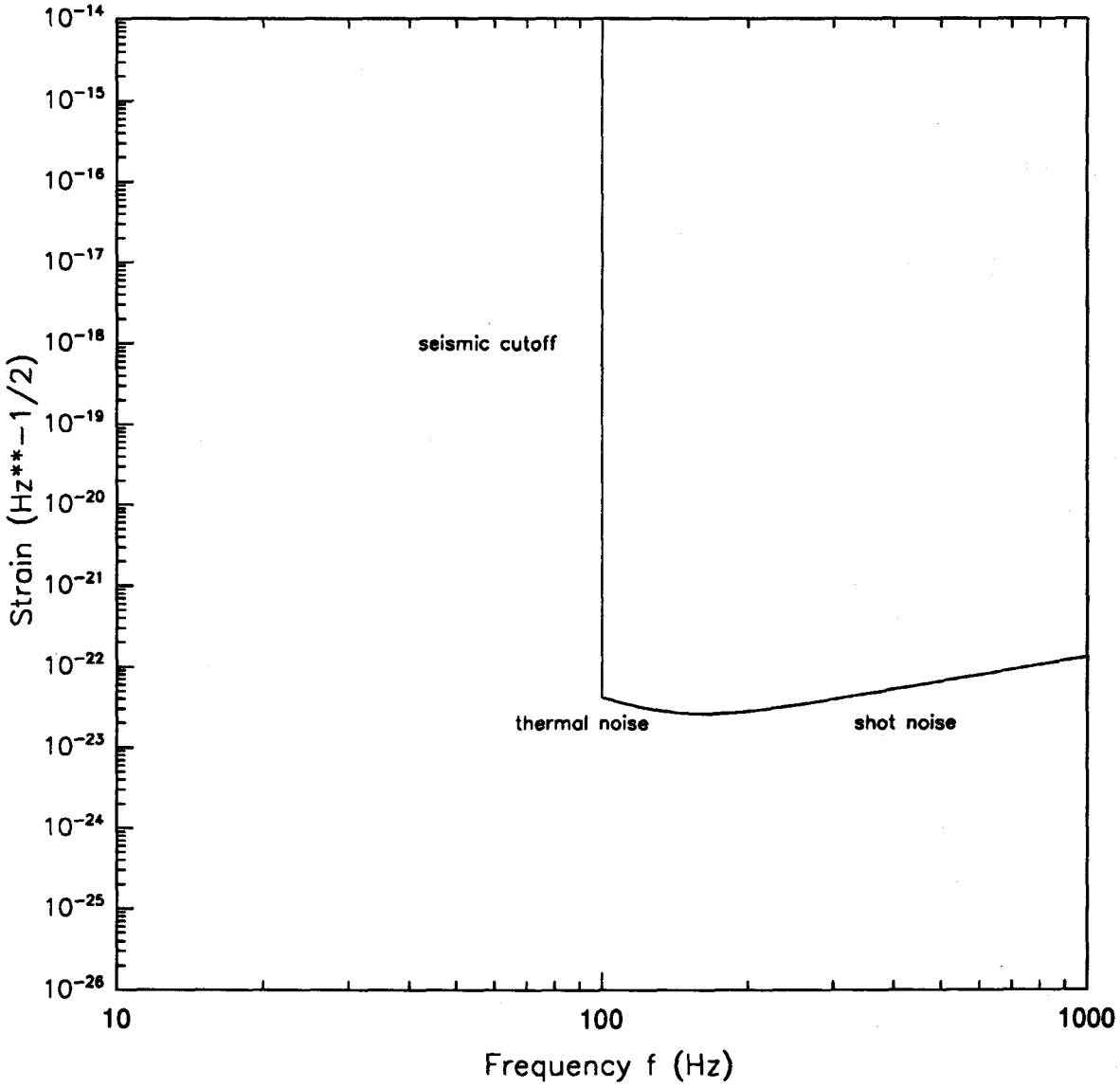

Figure A.1. Model strain contributions due to interferometer seismic, pendulum thermal, and photon shot noise for seismic cutoff frequency f_c = 100 Hz, effective pendulum quality factor $Q_e = 10^7$, and effective laser power P_e = 2 Watts.

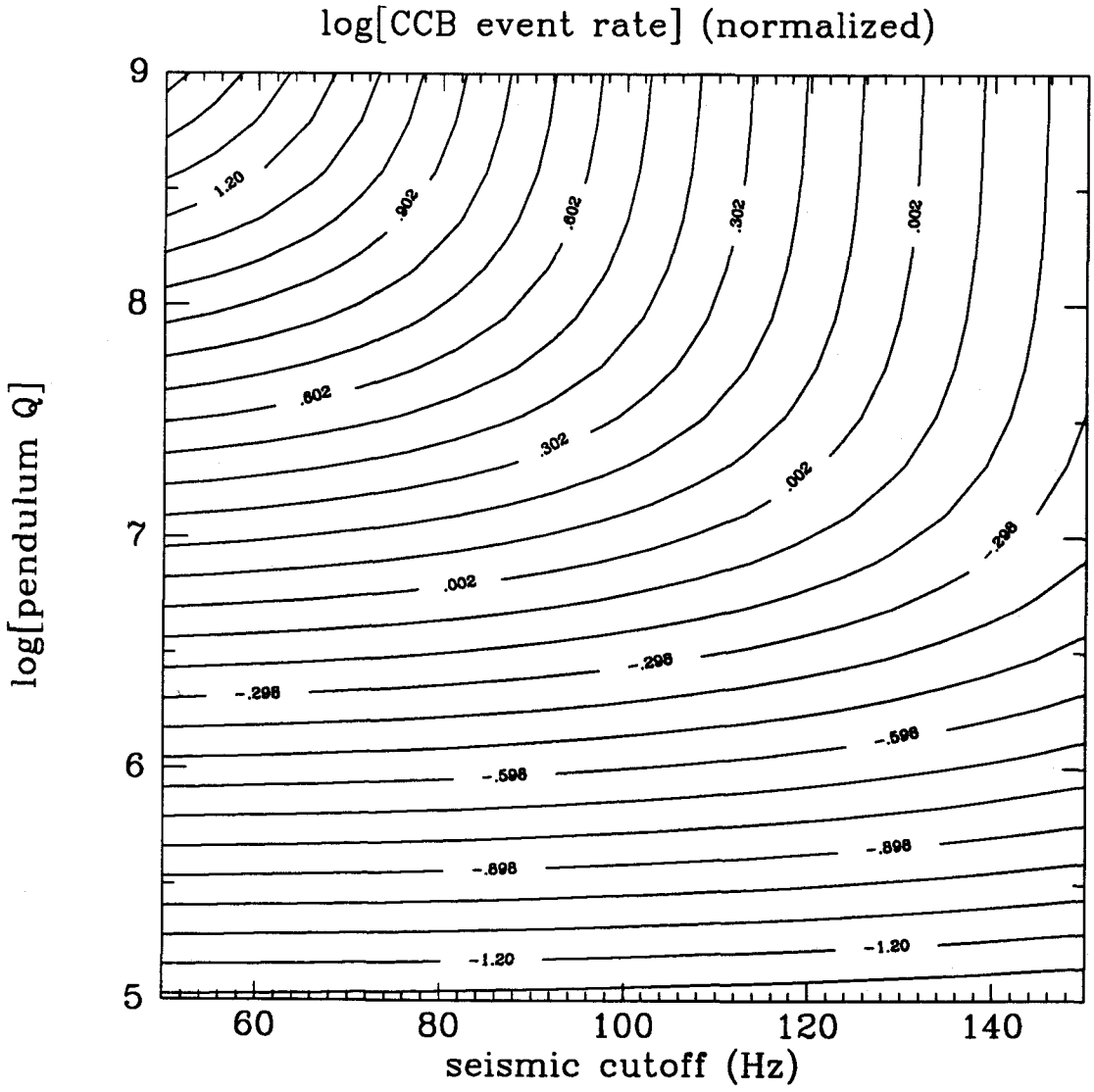

Figure A.2. Relative neutron star coalescence event detection rate as a function of receiver seismic cutoff frequency f_c and effective pendulum quality factor Q_e, for fixed effective laser power P_e = 2 Watts.

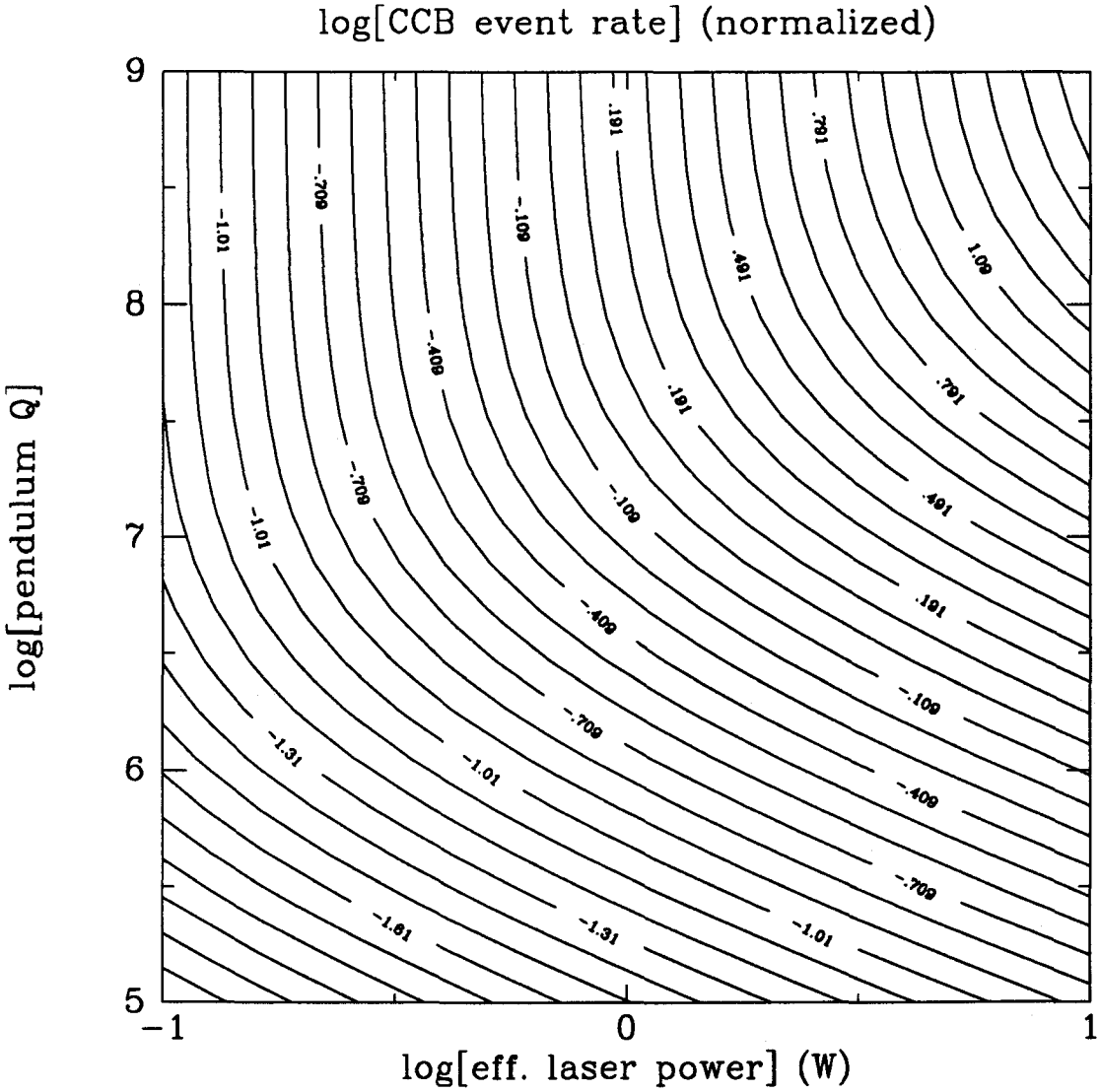

Figure A.3. Relative neutron star coalescence event detection rate vs. effective pendulum quality factor Q_e and effective laser power P_e = 2 Watts, assuming a fixed seismic cutoff frequency f_c.

Bibliography

[1] *NSF Proposal: A Laser Interferometer Gravitational-Wave Observatory.* December 1989.

[2] A. Abramovici. "Phase, Displacement, h Sensitivity for Recombined Fabry-Perot Interferometers". Notes from A. Abramovici May 3, 1992.

[3] A. Abramovici, W. E. Althouse, R. W. Drever, Y. Gursel, S. Kawamura, F. J. Raab, D. Shoemaker, L. Sievers, R. E. Spero, K. S. Thorne, R. E. Vogt, R. Weiss, S. E. Whitcomb, and M. E. Zucker. "LIGO: The Laser Interferometer Gravitational Wave Observatory". *Science*, 256:325–333, April 17, 1992.

[4] Brillet. Personal communication to D.H. Shoemaker.

[5] J. Chapsky, A. Abramovici, et al. File on Electronics for Modified Spectra Physics Laser. This file contains the circuit diagrams and transfer functions for the electronics used to control the modified spectra physics laser. It needs to be reviewed and updated so that the information is in a form that can be handed over to an engineer to build. The file is presently in the hands of Jake Chapsky.

[6] J. Giaime, P. Saha, D. Shoemaker, L. Sievers, and R. Weiss. "Passive Vibration Isolation for LIGO Interferometers: Modeling, Design, and Experimentation". *Rev. Sci. Instruments*, To be published.

[7] L. Jones, A. Abramovici, et al. File on the Modifications to Spectra Physics Laser. This file contains mechanical and optical layouts, part numbers, drawings, etc. for the modified prestabilized spectra physics laser. It needs to be reviewed and updated so that the information is in a form that can be handed over to an engineer to build. The file is presently in the hands of Doug Jungwirth.

[8] L. Jones and L. Sievers. "Interferometer Access Considerations and Optical Component Layout". Sept 1992. LIGO Working Paper #?

[9] J. Kovalik. Proposal for experiment on thermal noise. 1990.

[10] M. Regehr. Private communication to R. Spero, May 11, 1992.

[11] P. Saulson. "Thermal Noise in Mechanical Experiments". *Physical Review D*, 42(8), October 15, 1990.

[12] D. H. Shoemaker. "Considerations of the RMS motion of the LIGO cavity mirrors". 1992. LIGO Working Paper #109.

[13] D. H Shoemaker, P. Fritschel, J. Giaime, N. Christensen, and R. Weiss. "Prototype Michelson Interferometer with Fabry-Perot Cavities". *Applied Optics*, **30**(22):3133–3138, August 1991. Equation 2 includes a factor of 2 correction to the formula presented in this paper, communicated to R. E. Spero by D. Shoemaker May 11,1992.

[14] L. Sievers. "Notes on LIGO Stack Transfer Functions: Calculations and Assumptions". to be written. LIGO Working Paper #?

[15] K. S. Thorne. "Gravitational Radiation" in *300 Years of Gravitation.* Cambridge University Press, Cambridge, 1987. pages 330–458.

[16] R. Weiss and D. Shoemaker. "Analysis of an Externally Modulated Recycled Interferometer". Summary sent to Caltech May 6, 1992. Equations on page 15 most relevent.

BATCH START

STAPLE
OR
DIVIDER

Caltech
California Institute of Technology
Pasadena, CA 91125

ligo memorandum

TO: Distribution

DATE: 12 October, 1990

FROM: M. E. Zucker, D. H. Shoemaker

MAIL STOP/TELEPHONE: 130-33/4017

FILE: ~mike/iicd/handbook/hbookv1.tex

SUBJECT: LIGO INTERFEROMETER CONCEPTUAL DESIGN DOCUMENT

Attached is the first installment (Draft Version 1.04) of the *LIGO Interferometer Conceptual Design Handbook.* Your comments and suggestions will be appreciated, if possible well in advance of the next LIGO monthly review. Please bear in mind that this document is merely a beginning to the conceptual design process, and should be considered incomplete and tentative.

MEZ

Distribution:

A. Abramovici
W. Althouse
J. Chapsky
R. Drever
Y. Gürsel
S. Kawamura
R. Prout
F. Raab
R. Spero
R. Vogt
R. Weiss

FILE copy
NOTEBOOK (2) copies

LIGO Interferometer Conceptual Design Handbook

D. H. Shoemaker[1] M. E. Zucker[2]

12 October 1990

[1]LIGO, Massachusetts Institute of Technology
[2]LIGO, California Institute of Technology

Contents

List of Figures

Chapter 1

Introduction

1.1 Purpose and Strategy

file purpose.tex, 10/12/90

This document is a resource for conceptual design of LIGO interferometers. In the first chapter, the point of departure for the design is briefly mentioned: the specifications for the interferometer as a whole, similar to those described in the 1989 LIGO constructon proposal [2], and the departures from that model.

The second chapter describes the design in functional terms. A top-level breakdown of the interferometer into functional systems is presented as a block diagram. Each one of these top-level systems is then presented at a higher level of detail, with a page of text which describes the subsystem. More detailed diagrams describing subsystems of each system will eventually be produced; an example (for one of the better–defined subsystems) is included in this release.

The goal of the of the current effort is to create the framework that will help the science and engineering teams organize their efforts and thus put the necessary design information on a firm, buildable basis. There are some areas (laser stabilization, component isolation and suspension) where enough detail is already known to make useful designs and specifications. Most other aspects of the interferometer design will take significant amounts of additional research.

1.2 Base Design

file basedesign.tex, 9/26/90

The base design outlined here is intended only to focus the design effort, and should not be considered permanent or exclusive. As more substantive information becomes available we anticipate significant evolution of interferometer performance goals and of the design features needed to achieve them. Nevertheless, communication and cooperation in the design process demand an accepted and agreed–upon common basis, which at any given time should reflect a reasonable consensus of the interferometer design team.

This section should in future contain the kind of noise budget predictions and coarse overall diagrams of the interferometer configuration, like in the constru proposal

1.2.1 Performance Goals

file perfgoals.tex, 10/12/90

The overall LIGO interferometer specifications are taken to be those in [2], pages 43–51. To summarize, the circulating light power and cavity finesse will be sufficient to achieve a shot-noise limited strain sensitivity at 50 Hz of $10^{-23}/\sqrt{\text{Hz}}$. The filtered seismic noise will not compromise the shot noise limited sensitivity [3] for frequencies greater than 100 Hz. The thermal noise due to the pendulum mode of the test-mass suspensions will be below the shot noise limited sensitivity for frequencies greater than 200 Hz. Other sources of noise, including radiation pressure [4], fluctuations in the optical path due to residual gas [5], thermal noise due to internal mass modes [6], and noise due to imperfections in the illuminating light (frequency, amplitude, and beam motion) will each contribute less than the shot, seismic, and thermal noise so that the sum of their influences does not significantly compromise the strain sensitivity.

1.2.2 Assumptions and Basic Design Decisions

file assumptn.tex, 10/12/90

The proposed basic design also closely follows the design outlined in the 1989 LIGO proposal. Light from a single Argon ion laser illuminates a Michelson interferometer [7]; the laser output power will be 5 W, and the overall optical efficiency of the system will be 0.2. A not–yet–determined combination of single–mode fibers and resonant Fabry–Perot cavities used in transmission [8] will be used to stabilize the frequency, amplitude, position and direction of the light. The Fabry–Perot cavity in each arm of the interferometer will have a storage time of roughly 2 ms. Broadband recycling will be used to increase the circulating light power by a factor of 30. The differential phase

shift induced by gravitational strain will be detected by interfering the light from the Michelson beamsplitter's antisymmetric output port with a phase modulated reference beam, derived from the illuminating light, in an external Mach–Zehnder interferometer arrangement[1]. A system of automated optical alignment will be intrinsic to the design. A passive isolation stack employing unencapsulated elastomer springs will be used as the primary seismic isolation. Pendulum suspensions will be used for the optical components, with active damping and steering from local sensors and drivers. An instrumentation system will monitor and control adjustable parameters of the system.

Many basic design decisions have not yet been made. The correct combination of "mode cleaners" (input laser beam conditioners) must be determined. The techniques for obtaining the resonance condition of the main Fabry-Perot cavities, the recycling cavity, the Michelson interferometer, and the strain-readout interferometer are not yet specified. The specific method of obtaining the error signal for the auto-alignment system is not yet determined. The test mass suspension is a special case, and its overall form and sensing/driving technology have yet to be determined. Research programs attempting to answer these and other open conceptual design questions are outlined in Appendix B.

[1]This differential phase detection method represents our principal departure from the system described in [2]

Chapter 2

Functional Breakdown of Subsystems

2.1 Major Systems

file majsys.tex, 10/5/90

Figure 2.1 is a functional breakdown of the proposed design. This presentation, as opposed to a breakdown in terms of categories (optics, electronics, control, etc.), is chosen because it appears to be the simplest way to describe the design. The numbers (icd100, etc.) can be a point of departure for a work-breakdown structure. At this level the Data and Control System interfaces are not yet explicit.

The second level of functional breakdown is shown in the series of figures (Figures 2.2, 2.4, etc.), and in specification lists that follow in Section 2.2.

Many categories are not yet complete. In particular ICD1000 thru ICD1300 do not yet have firm configuration concepts; the diagrams for those systems are currently left blank

Figure 2.3 is an example of a third-level breakdown. The units depicted on this diagram are each intended to be at the complexity level of an individual electronic module or optical assembly. The next (and probably the final) breakdown level should then comprise detailed mechanical drawings, electronic schematics, assembly diagrams and parts lists.

2.2 Subsystems and Specifications

file subsys.tex, 10/11/90

In this section each system identified in Figure 2.1 is described by a list which tersely summarizes the state of the design team's knowledge for that system. Each system is then further broken down in a diagram depicting its own component subsystems and their functional interrelationships. The subsystems themselves may be further broken down into component–level diagrams, at the level of electronic modules or individual optical components. This has been done for subsystem ICD111, the laser stabilizing servo electronics, in Figure 2.3. Finally, engineering documentation, including circuit diagrams, mechanical drawings, detailed optical specifications, and parts lists, will be provided for each module or component.

A sample system specification list explaining the entries, and a glossary of abbreviations found in the specification lists, are included here for reference.

Sample System Specification List

UNIT: ICDXYZ Identification and title

REV: Last revision date, author, maybe nature of revisiton, perhaps some other notes about previous revisions, etc.

SCOPE: One or two paragraphs describing the system. Initially, it is a list of parameters that must be specified; later, the numerical values should be inserted. If a trivial test procedure exists for verifying that the unit meets a certain specification, it is indicated with an (ok) in parenthesis. If a few-word description of a test procedure is possible, it is indicated in parenthesis. For more difficult test procedures, or where the test procedure has not yet been determined, see the entry under the TEST heading.

SPECS: List of things that should be determined to initiate design of this thing

PREREQS: Other units at this level which should provide some needed input for this unit's spec

RELATED: Units whose designs will need to evolve at the same time as this unit, because they are seriously interrelated

TEST: Nonobvious, subtle, or highly critical features which must be tested and/or evaluated to qualify for use (or whose untestability may force the design)

DCS I/O: Signals supplied to and required from the data and control system.

Glossary of Abbreviations

FP: Fabry-Perot cavity. When used as a test device, can either give an analysis of the spatial modes incident on the FP, or measure the frequency fluctuations in the incident light.

PD: Photodiode

QPD: quadrant PD, 4 closely spaced photodiodes, giving X and Y (in the photodiode plane) beam position information

CCD: Charge Coupled Device, here used for a solid-state imaging device (TV camera). A Beam Analysis Device is something which allows a quantitative analysis of an image from a CCD.

RF: unless otherwise stated, a high frequency ($\approx$10 MHz) modulation voltage or detection signal

FSR: Free Spectral Range of a Fabry-Perot cavity

BAD: Beam analysis device; something which allows a quantitative analysis of an image from a CCD.

Wyko: A test interferometer that can measure the figure of (also large) test pieces

LIGO: used to indicate the installed LIGO interferometer, as opposed to a prototype scale instrument

XF: transfer function, either optical, mechanical, or electrical. Also applies to general (nonlinear, nonorthogonal) cases where appropriate.

MZ: Mach–Zehnder; the optical interference configuration used to read out the phase change in the output from the Michelson interferometer as part of the Differential Phase Detection system.

2.2.1 ICD100 Laser Prestabilization

file icd100.tex
10/9/90

UNIT: Laser Prestabilization System

REV: DHS 22 July 90

SCOPE: ICD100 includes the laser(s) and associated electronics, and an initial frequency stabilization to a short rigid FP reference cavity. Active power stabilization will probably also be necessary. It is based on a commercal Argon laser, rebuilt to allow frequency stabilization. There may be several lasers with a change-over system.

STATUS: Extensive prototype experience with Argon lasers. Close to transfer to engineering

SPECS:
(a) average power (power meter)
(b) duty cycle (ok)
(c) changeover time (ok)
(d) power fluctuation spectrum (fast PD)
(e) lowest shot-noise limited frequency (fast PD)
(f) frequency noise spectrum (ext. FP measurement cavity)
(g) pointing stability in position and angle, fluctuation spectrum (QPD)
(h) output beam waist and position (FP or CCD + BAD)
(i) power in fundamental spatial mode

PREREQS:

RELATED:

TEST: Existing procedures

DCS I/O: In: lock/unlock (10 Hz). Out: servo status, error, control (10 kHz), alignment status (10 Hz)

ICD111 Laser Stabilization Servo Electronics

The prestabilized laser system, ICD100, uses this electronics package, depicted schematically in Figure 2.3, to control and monitor the laser wavelength and power. ICD111 is also the principal contact point for Data and Control System interaction with the laser system. The DCS interface connections (shown as numbered double arrows in Figure 2.3) are identified as follows:

Data and Control System Interface Legend
ICD111, Laser Stabilization Servo Electronics

111a Power Stabilizer Servo Electronics

IN: Mode (Run,Protect,Test,...), Operating Point, Max. Level, Min. Level

OUT: Feedback Signal, Error Signal, Status

111b Master RF Oscillator

IN: Run/Idle/Test, Freq. Select

OUT: Oven Temp., Output Level, Status

111c RF Power Amplifier

IN: Run/Idle/Test, Gain

OUT: Output Level, Load SWR, Status

111d RF Phase Shifter

IN: Run/Idle/Test, Phase Set

OUT: Input Over/Under Range, Status

111e Photodetector Interface Module

IN: R/I/T, Range, BW, Protect Mode, Bulb Current

OUT: DC Photocurrent, Bias V, RF Ovld., DC Ovld., Substrate Temp., Status

Data types and bandwidths, as defined in Chapter 4 for example, should be added to the 'in' and 'out' lists of each component.

111f RF Preamplifier

IN: R/I/T, Gain, Acq./Run

OUT: Ovld., Status

111g Mixer/Video Preamplifier

IN: R/I/T, Video Gain, Acq./Run

OUT: LO Over/Under Range, RF Ovld., Status

111h AGC Sensor

IN: R/I/T, Sensitivity, Hold

OUT: AGC Err. Sig., Over/Under Range, Status

111i Fast Servo Electronics

IN: R/I/T, Run/Acq., Gain

OUT: Ovld., Err. Sig. Mon., Status

111j Auto Fringe-Hop Controller

IN: R/I/T, Seek, Up(n)/Down(n), Delta, Threshold

OUT: HV FB Level, Elapsed Time, Uncontrolled Hop, Hop Count, Hop Request, Status

2.2.2 ICD200 Prefilter/Mode Cleaner

file
icd200.tex,
10/12/90

UNIT: Prefilter—mode cleaner

REV: 22 July 90

SCOPE: ICD200 Prefilter and mode cleaner performs the initial filtering of spatial beam motion, and the beam relaying from ICD100 to ICD300. It may take the form of a single-mode optical fiber or a Fabry-Perot cavity; polarization control and monitor may be needed.

SPECS:
(a) XF, beam motions x, y, θ_x, θ_y
(b) XF for input beam motions to output intensity changes
(c) XF for input to output frequency fluctuations
(d) optical throughput (PDs before and after)
(e) output polarization state and stability (polarization analyzer)
(f) output beam diameter and waist (ext. FP or CCD+BAD)
(g) % of power in fundamental mode (ext. FP)
(h) input and output isolation

PREREQS: ICD100 Laser specs. and ICD400 interferometer input prerequisites must be developed so that the criteria for sufficient isolation can be determined.

RELATED:

TEST: A testing device capable of generating a beam with periodic position and angular displacement but which generates a minimum of incidental frequency or amplitude modulation needs to be developed.

DCS I/O: Out: servo status, error, control signals (10 kHz), alignment status (10 Hz); In: lock/unlock (10 Hz)

2.2.3 ICD300 Input Mode Cleaner

file
icd300.tex,
10/4/90

UNIT: Input mode cleaner

REV: DHS 22 July 90

SCOPE: ICD300 Input mode cleaner serves as a filter for amplitude and frequency fluctuations and as a secondary frequency reference. It may also serve to reduce position fluctuations in the beam depending on the efficiency of ICD200. Extensive laboratory experience with FP's. FP's with hanging mirrors, used in transmission as mode cleaners, have not been explored experimentally. Multiple frequency references have been used elsewhere; servo-loop topologies must be refined.

SPECS:
(a) output frequency noise (ext. FP)
(b) output power flucuation noise (fast PD)
(c) beam pointing stability, long- and short-term (QPD)
(d) power handling capability (power meter, high P laser, FP)
(e) optical throughput (PDs before and after)
(f) storage time

PREREQS:

RELATED:

TEST: Existing procedures

DCS I/O: Out: servo status, error, control (10 kHz), alignment status (10 Hz); In: lock/unlock (10 Hz)

2.2.4 ICD400 Interferometer Injection

file icd400.tex, 10/4/90

UNIT: Interferometer injection

REV: DHS 22 July 90

SCOPE: ICD400 Interferometer injection consists of the steering and matching optics used to couple the light from the fore-optics (ICD100—ICD300) into the main interferometer.

SPECS:
(a) input beam parameters
(b) range of output beam parameters (CCD+BAD)
(c) beam distortion (Wyko? TBD)
(d) power handling capability (Wyko + high power laser)
(e) optical throughput (PDs before and after
(f) resolution of adjustment; mechanical disturbance due to adj. (ok)
(g) matching precision, i.e., power coupled into TEM_{00} mode (Wyko?)

PREREQS:

RELATED:

TEST: Commercial interferomter (Wycko) and/or FP cavity to analyze beam quality for large beams is needed.

DCS I/O:

2.2.5 ICD500 Recycling

file icd500.tex, 10/4/90

UNIT: Recycling

REV: DHS 22 July 90

SCOPE: ICD500 Recycling includes the recycling mirror and its suspension, locking, and orientation system, and the modulation which precedes the interferometer. These modulators may be before the ICD400 injection expansion telescope. A simple fixed-reflectivity recycling mirror is proposed.

SPECS:
(a) optical beam matching to 4 km interferometer cavities ICD700,800 (?)
(b) surface figure (Wycko?)
(c) mirror (Rec. Mirror) transmission (PD)
(d) recycling mirror losses (?)
(e) modulation depth (ext. FP)
(f) beam distortion due to substrate, also as a function of power (Wycko?
(g) deviation from resonance of the recycling cavity (LIGO)

PREREQS:

RELATED:

TEST: Method for the determining mirror figure and substrate distortion, fine and large scale, needs to be developed.

DCS I/O: In: modulation depth (10 Hz), lock on/off (10 Hz), alignment (TBD); Out: status (10 Hz)

2.2.6 ICD600 Michelson

file
icd600.tex,
10/8/90

UNIT: Michelson Interferometer

REV: DHS 18 June 90

SCOPE: ICD600 Michelson includes the main Michelson beamsplitter, the pick-off for the Mach-Zehnder reference beam, and associated pointing and damping systems.

SPECS:
(a) contrast of Michelson interferometer as limited by ICD600 components (Wycko)
(b) maximum power (see below)
(c) pointing accuracy of reflected arm beam from 'left' cavity (QPD)
(d) pointing accuracy of MZ reference arm (QPD)
(e) fluctuation from dark fringe (LIGO)
(f) residual motion of components (small test ifo using ICD600 components)

PREREQS: ICD700, 800 arm cavities

RELATED:

TEST:

DCS I/O:

2.2.7 ICD700 Left Cavity

file
icd700.tex,
10/8/90

UNIT: Left Cavity

REV: DHS, 22 July 1990

SCOPE: ICD700, the left 4-km cavity of the interferometer, consists of the two cavity mirrors, their suspensions and isolation systems, and the alignment and locking sensors and drivers.

SPECS:
(a) storage time
(b) maximum difference of storage time, right arm-left arm
(c) input beam parameters
(d) maximum difference of beam parameters, right arm-left arm
(e) wavefront distortion of reflected beam on resonance
(f) maximum difference of reflected beam parameters, right/left
(g) visibility
(h) maximum difference of visibilities, right/left
(i) alignment stability, long term
(j) alignment stability, short–term
(k) maximum deviation from resonance
(l) power handling capability
(m) cavity lock duty cycle; time for re-locking

PREREQS:

RELATED:

TEST:

DCS I/O:

2.2.8 ICD800 Right Cavity

file icd800.tex, 10/8/90

UNIT: Right Cavity

REV: DHS, 9/22/90

SCOPE: ICD800, the right 4-km cavity of the interferometer consists of the two cavity mirrors, their suspensions and isolation systems, and the alignment and locking sensors and drivers.

SPECS:
(a) storage time
(b) maximum difference of storage time, right arm-left arm
(c) input beam parameters
(d) maximum difference of beam parameters, right arm-left arm
(e) wavefront distortion of reflected beam on resonance
(f) maximum difference of reflected beam parameters, right/left
(g) visibility
(h) maximum difference of visibilities, right/left
(i) alignment stability, long term
(j) alignment stability, short–term
(k) maximum deviation from resonance
(l) power handling capability
(m) cavity lock duty cycle; time for re-locking

PREREQS:

RELATED:

TEST:

DCS I/O:

2.2.9 ICD900 Differential Phase Detection

file
icd900.tex,
10/8/90

UNIT: Differential Phase Detection (formerly Mach-Zehnder)

REV: DHS 22 July 90

SCOPE: ICD900 comprises an external Mach-Zehnder (MZ) interferometer, consisting of a secondary beamsplitter, folding mirrors and electro-optic modulators. It provides the means for measuring the phase of the recombined "dark fringe" beam leaving ICD600, the Michelson interferometer, by combining this beam with a phase–modulated local oscillator beam derived before the ICD600 input.

SPECS:
(a) MZ fringe contrast
(b) MZ alignment stability
(c) MZ deviation from operating point
(d) residual motion of components
(e) modulation depth
(f) maximum power level
(g) path length equality
(h) backscatter to interferometer

PREREQS: 600 Michelson optics (for beam size)

RELATED: 1000 DPD control

TEST:

DCS I/O:

2.2.10 ICD1000 DPD Control

file
icd1000.tex,
10/8/90

UNIT: Differential Phase Detection Control

REV: DHS 18 June 90

SCOPE: ICD1000 contains the photodetectors, modulation and demodulation and servo electronics used to lock and hold the Mach-Zehnder interferometer of ICD900, the Differential Phase Detection System, at the proper reference phase and amplitude.

SPECS: (a) detection system noise

(b) deviation from 'dark' fringe

PREREQS: ICD900 Differential Phase Detection

RELATED: ICD110 MI control, ICD1300 Strain readout

TEST:

DCS I/O:

2.2.11 ICD1100 Michelson Control

file
icd1100.tex,
10/8/90

UNIT: Michelson Control

REV: DHS 16 June 90

SCOPE: ICD1100 Michelson Control is the fringe detection and servo system for the Michelson interferometer.

SPECS: (a) detection system noise

(b) deviation from 'dark' fringe

PREREQS: Locking plan; calibration scheme

RELATED: ICD1000 MZ control, ICD600 Michelson, ICD700, ICD800 Cavity Sytems

TEST:

DCS I/O:

2.2.12 ICD1200 Output Mode Cleaner

file
icd1200.tex,
10/8/90

UNIT: Output mode cleaner

REV: DHS 16 June 90

SCOPE: ICD 1200 Output mode cleaner selects the correct spatial mode from the output light from the interferometer, to improve the contrast and to eliminate scattered light. It may be a fiber or a Fabry-Perot cavity in practice.

SPECS:
(a) suppression of undesired modes
(b) optical efficiency
(c) alignment accuracy on the desired mode
(d) alignment stability on the desired mode
(e) noise contribution (mechanical or optical effects)
(f) locking system

PREREQS: scattering model; signal-to-noise calculation as a function of contrast; electro-optic power handling and wavefront distortion

RELATED: ICD200 Prefilter-mode cleaner, ICD300 Input mode cleaner

TEST:

DCS I/O:

2.2.13 ICD1300 Strain Readout

file
icd1300.tex,
10/8/90

UNIT: Strain readout

REV: DHS 18 June 90

SCOPE: Strain readout consists of photodetectors and protection circuits, demodulation circuitry, and possibly adding/differencing circuits which output a signal containing the strain information. Also included in this unit is the strain sensitivity calibration system.

SPECS: (a) detection system noise

(b) maximum incident power

(c) calibration accuracy (as a function of frequency)

PREREQS:

RELATED: ICD100 DPD control, ICD1100 MI control

TEST:

DCS I/O:

Interferometer conceptual design: Master block diagram

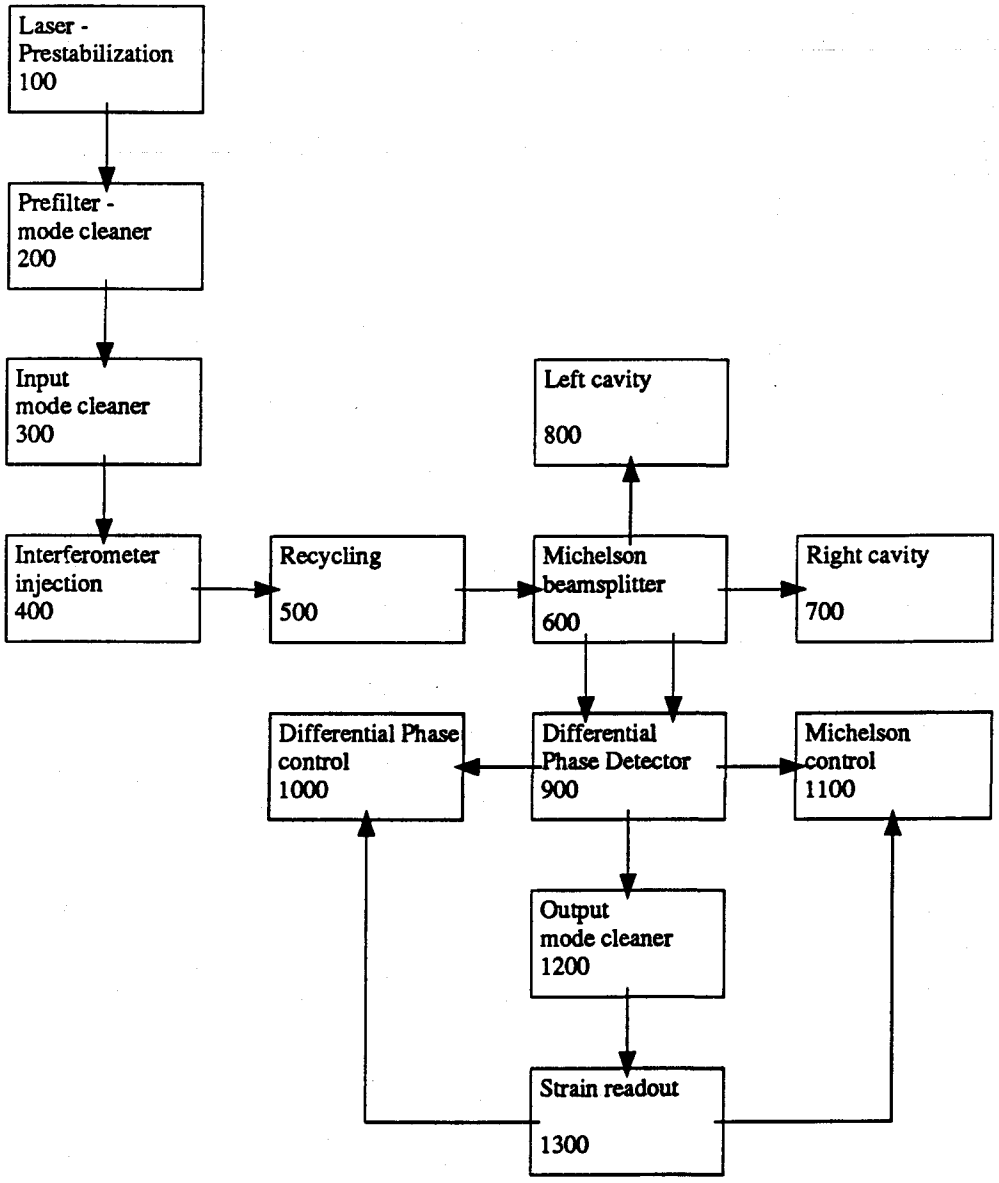

Figure 2.1: ICD000: Master Functional Block Diagram. Operational subunits of a LIGO interferometer are depicted, interconnected by major laser beam, signal flow and support interrelationships.

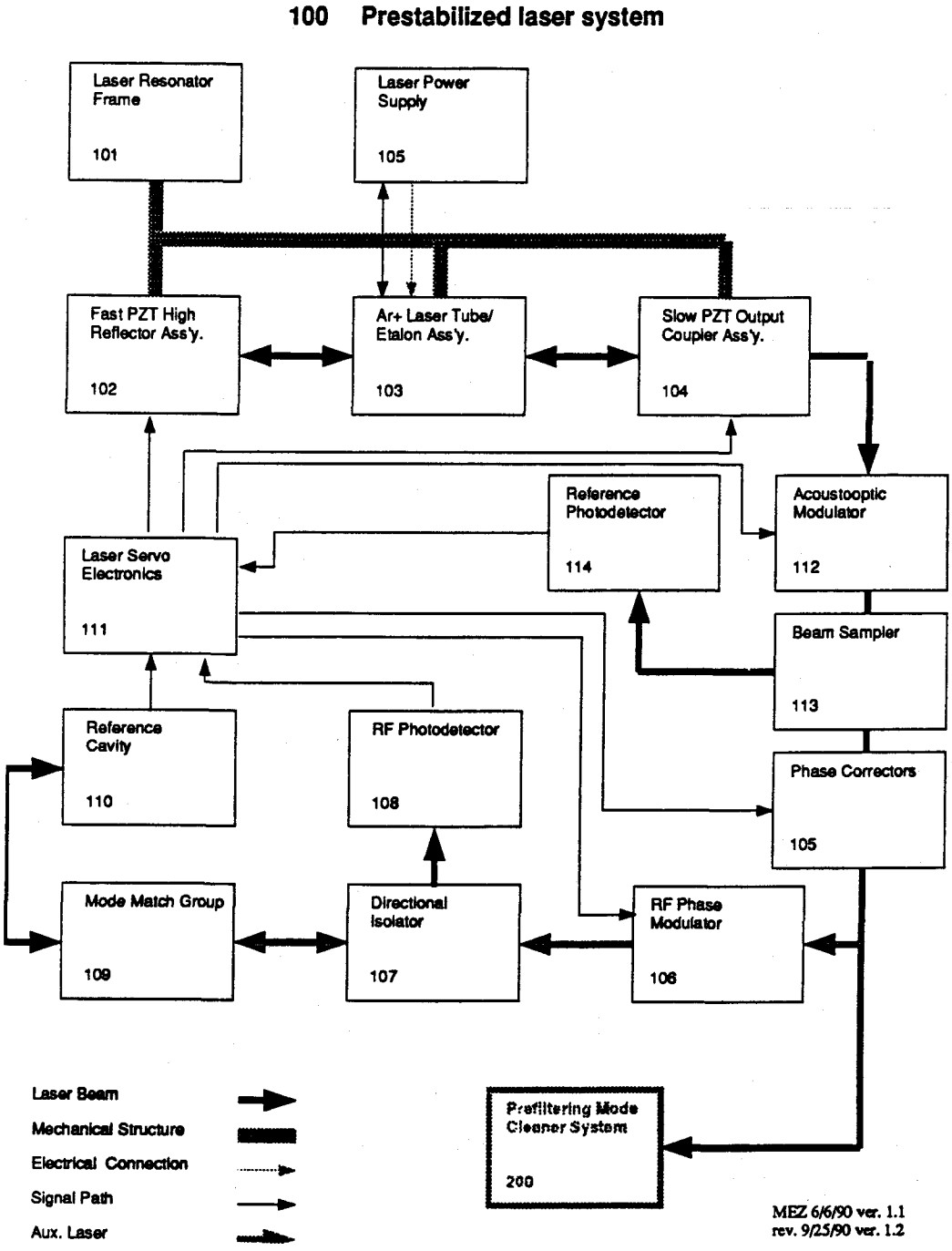

Figure 2.2: Block diagram of interferometer subsystem ICD100, the prestabilized laser system.

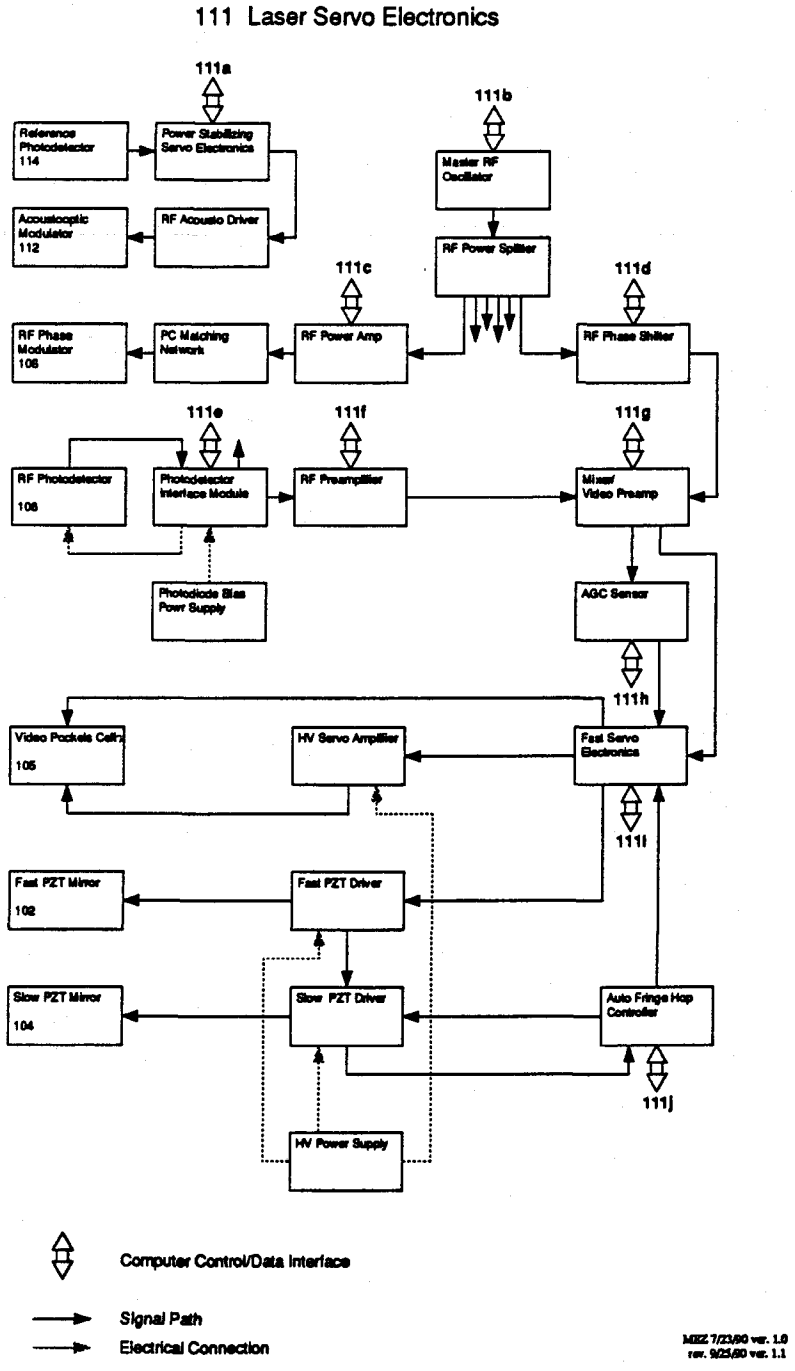

Figure 2.3: Subsystem ICD111 of interferometer system ICD100, the laser stabilization servo electronics package. Each unit shown is roughly the size and complexity of an electronic module or a mounted optical component, for example. Broad arrows indicate interfaces with the Data and Control System; the information carried by each interface is described in the text.

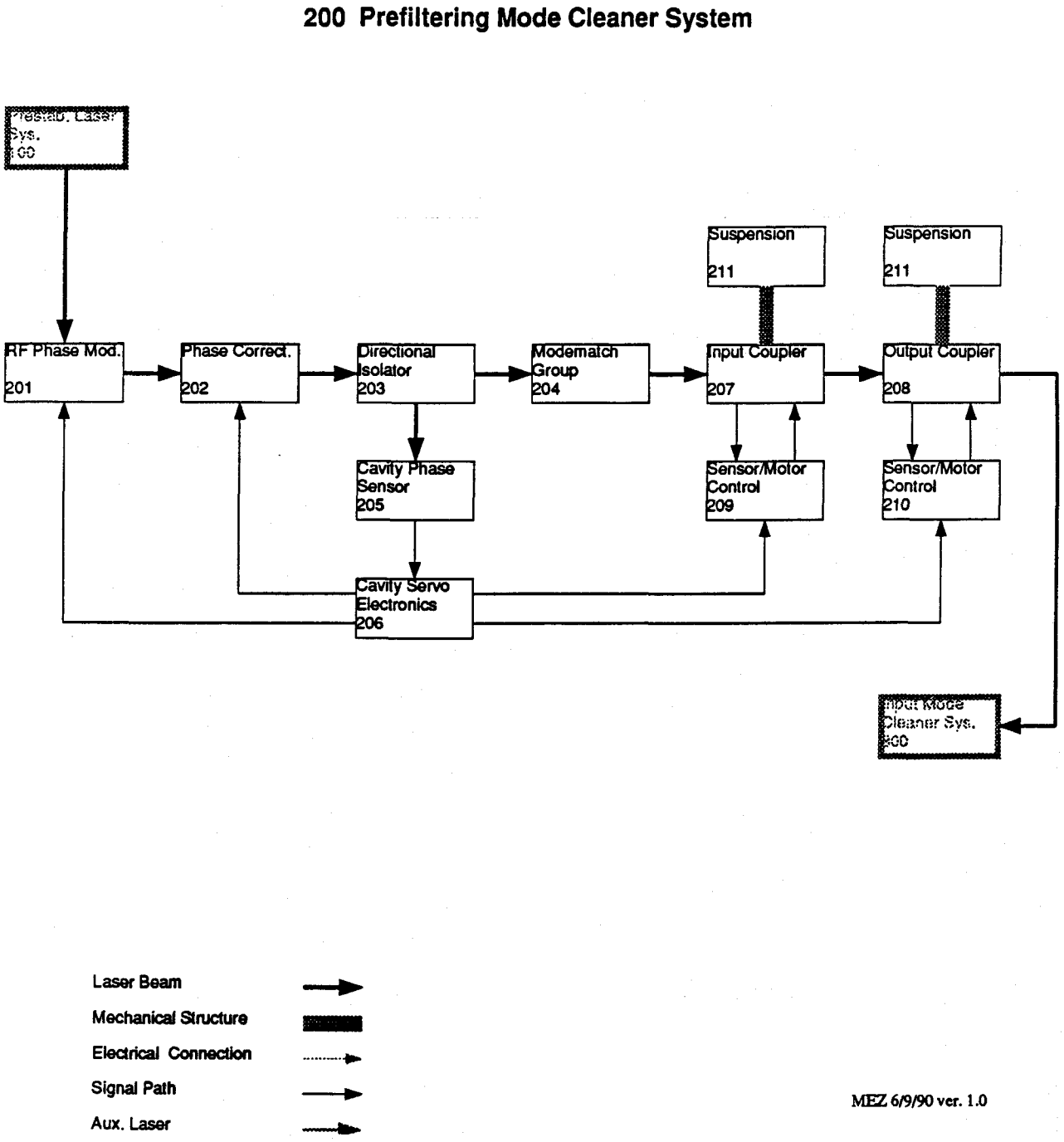

Figure 2.4: Block diagram of interferometer subsystem ICD200, the Prefiltering Mode Cleaner system.

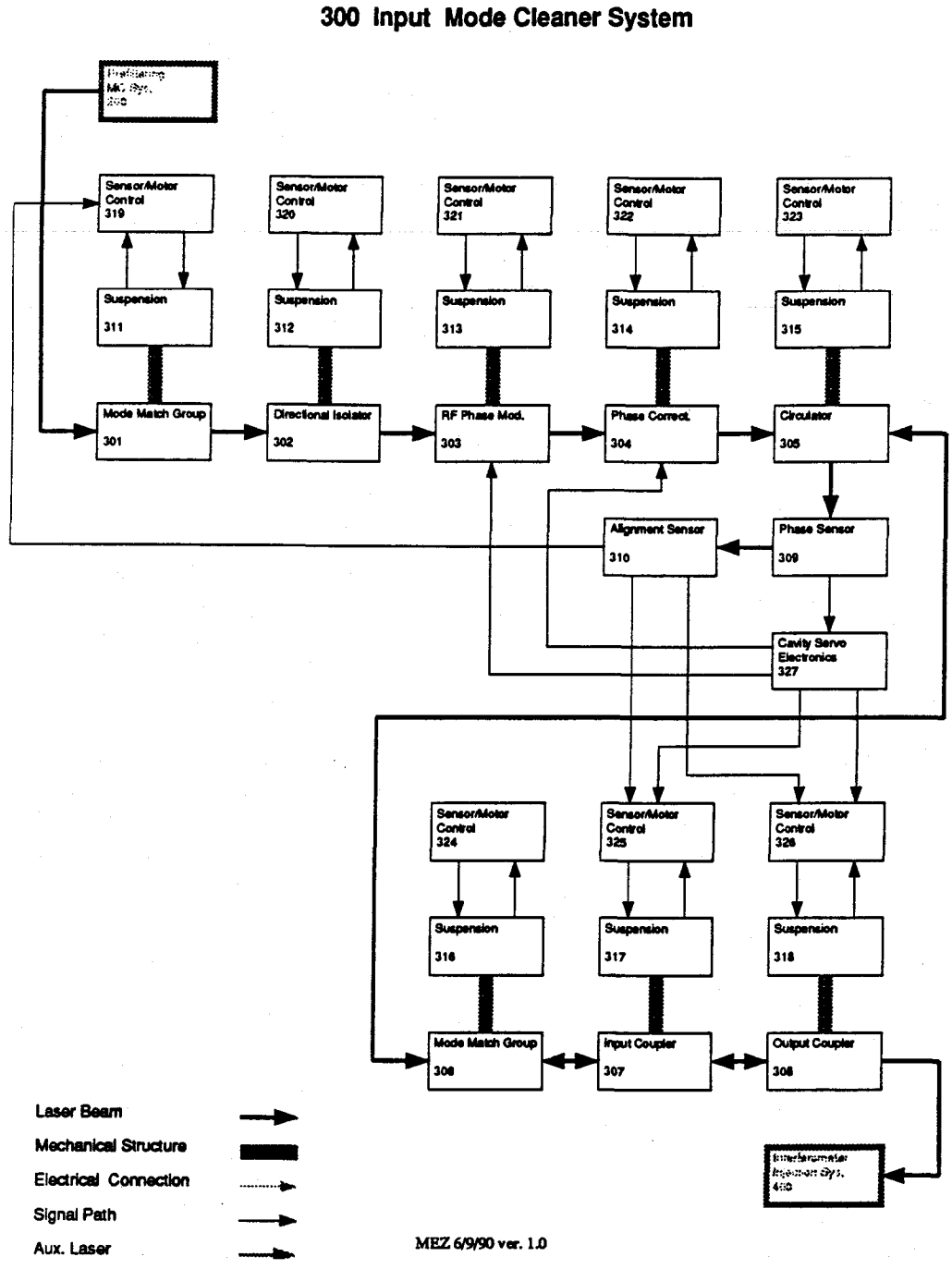

Figure 2.5: Block diagram of interferometer subsystem ICD300, the Input Mode Cleaner system.

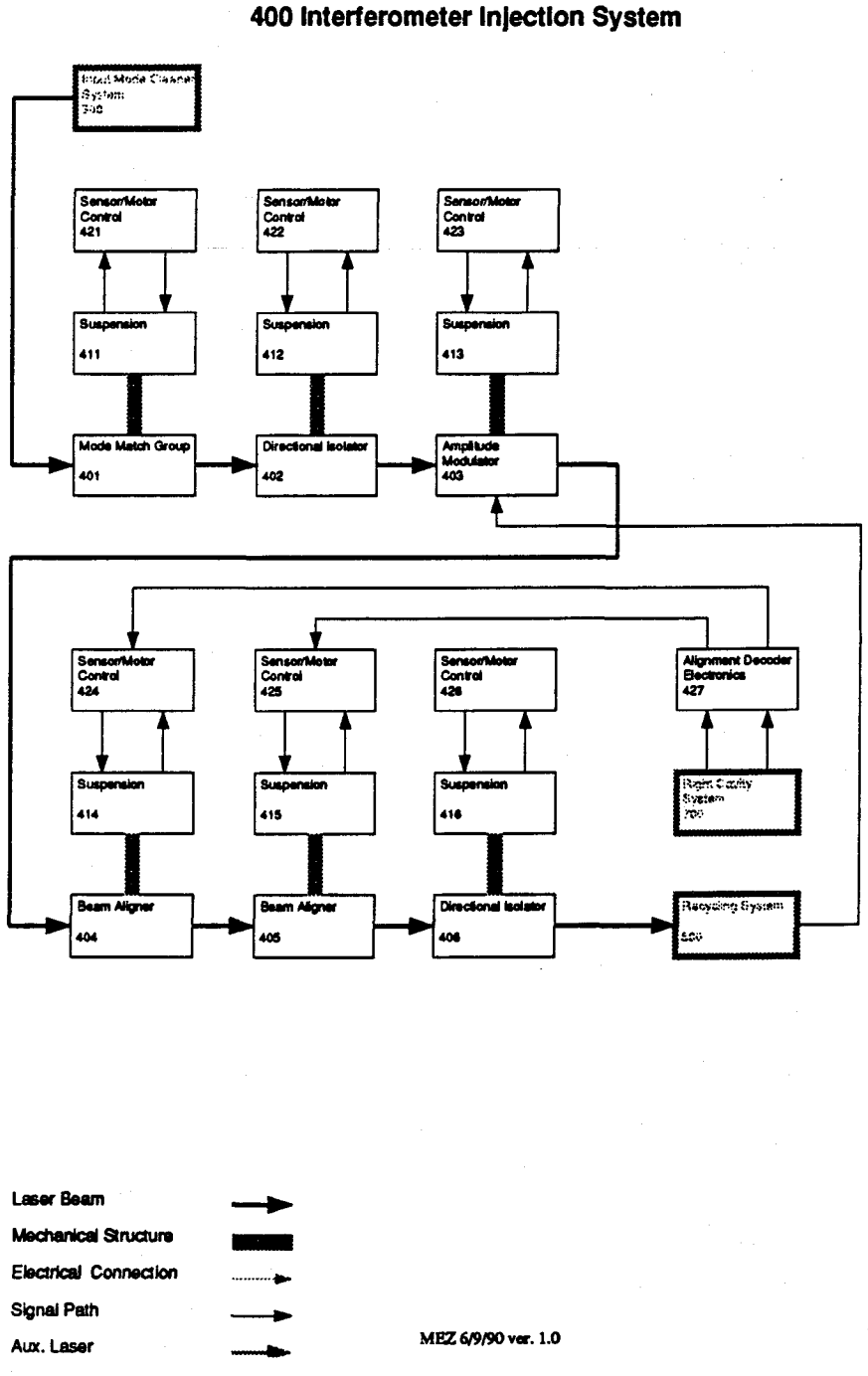

Figure 2.6: Block diagram of interferometer subsystem ICD400, interferometer injection.

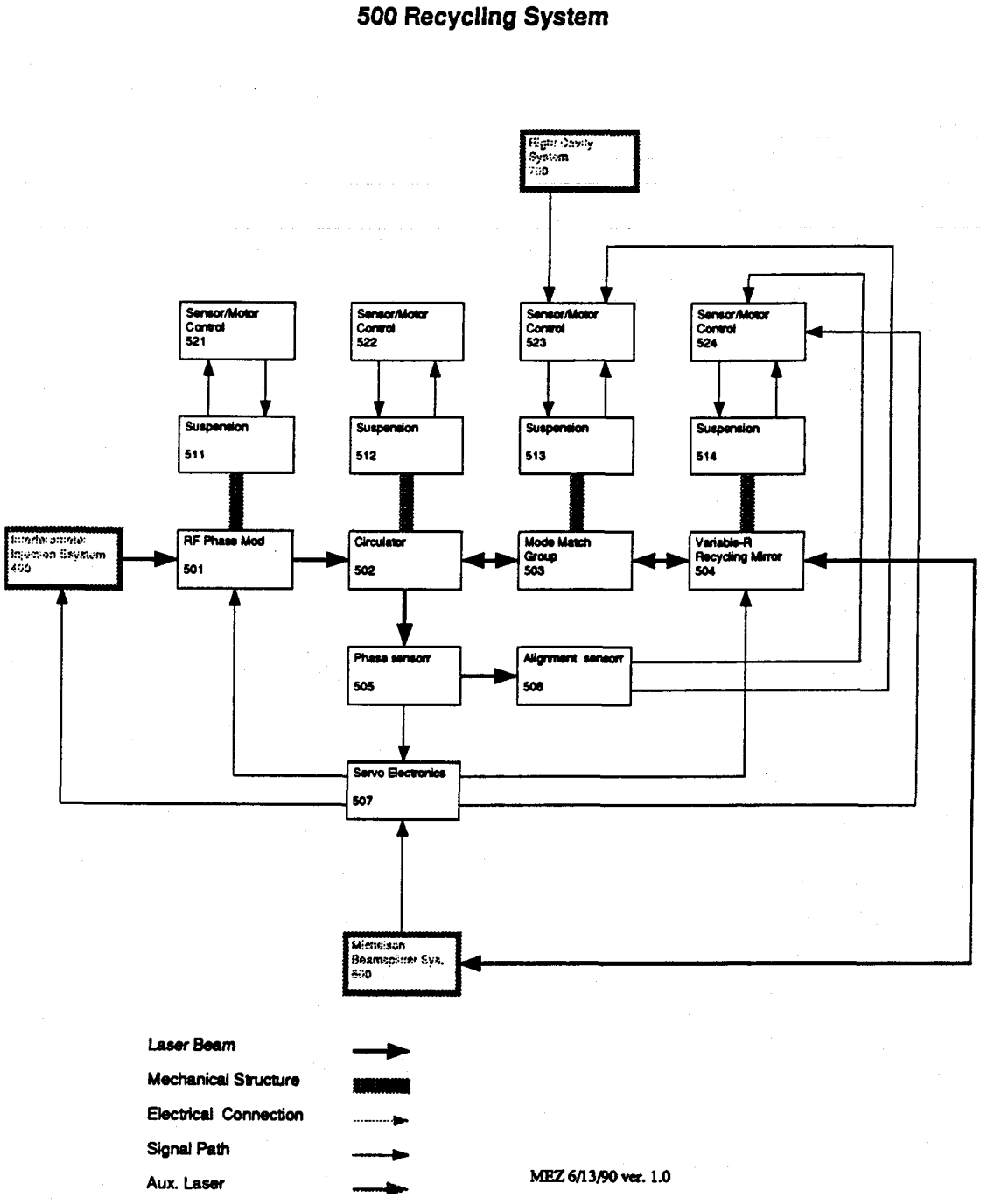

Figure 2.7: Block diagram of interferometer subsystem ICD500, recycling system.

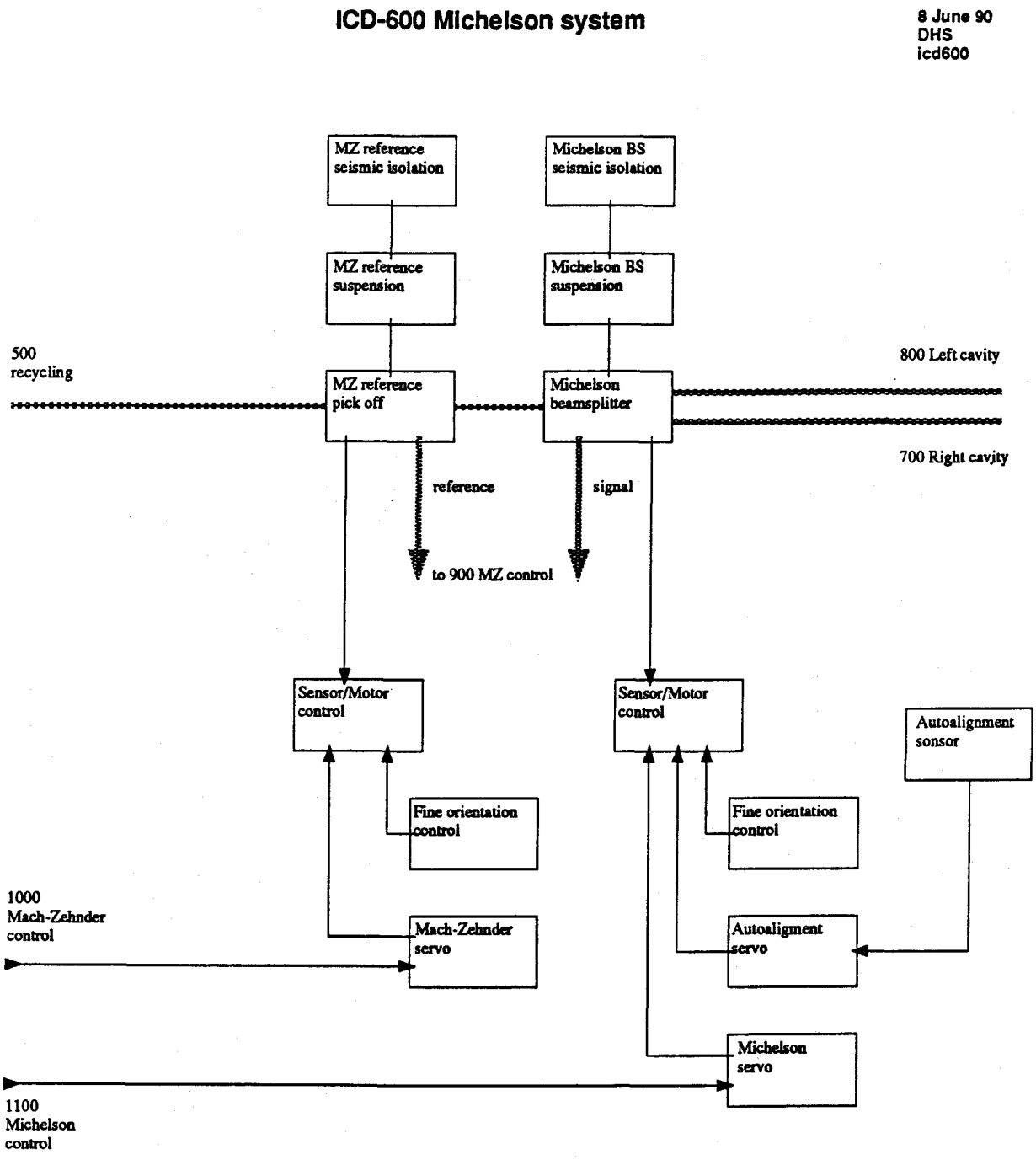

Figure 2.8: Block diagram of interferometer subsystem ICD600, Michelson system.

1 June 90
DHS, MEZ
icd700

ICD-700 Right cavity system

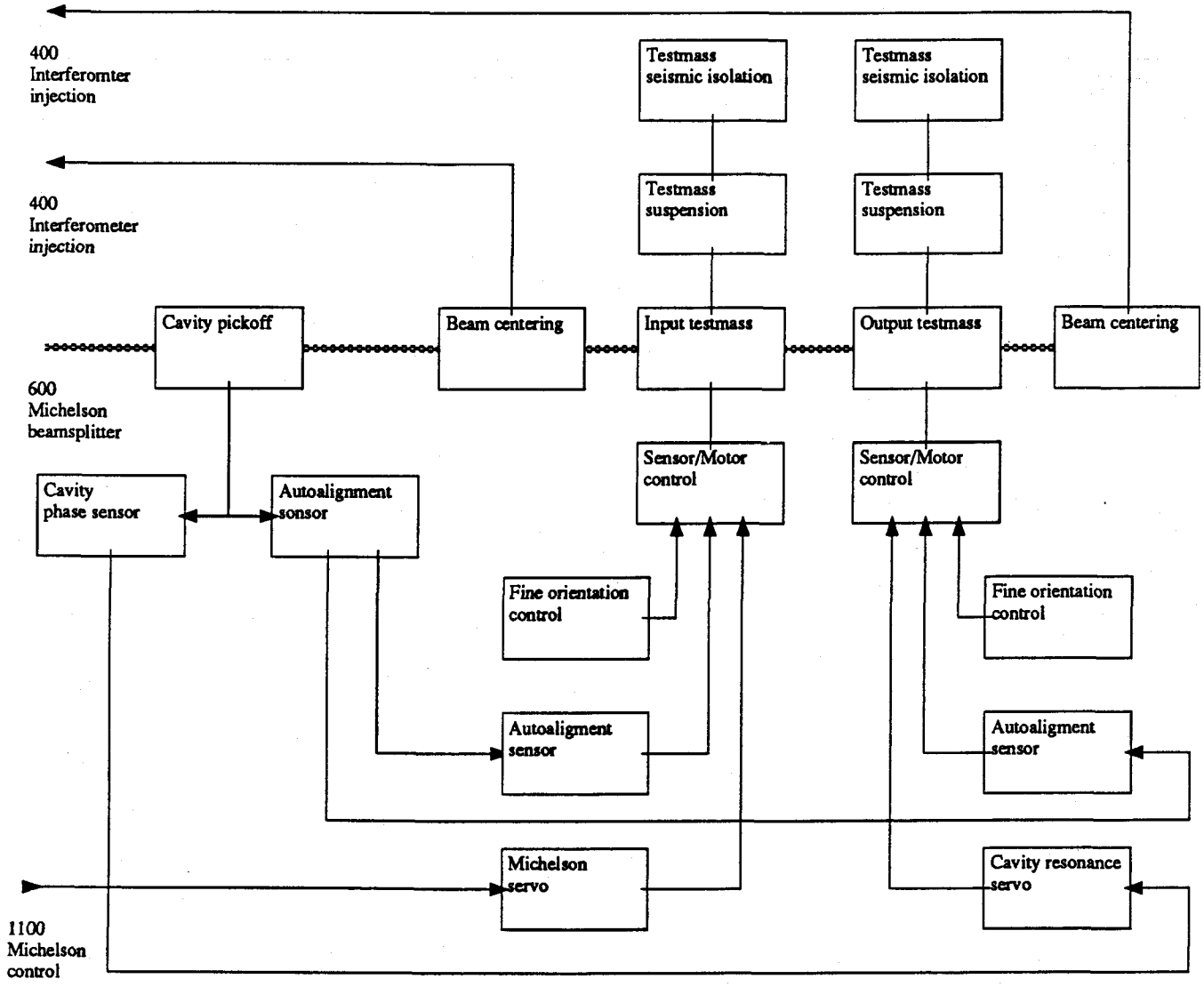

Figure 2.9: Block diagram of interferometer subsystem ICD700, the Left Cavity of the main interferometer.

6 June 90
DHS
icd800

ICD-800 Left cavity system

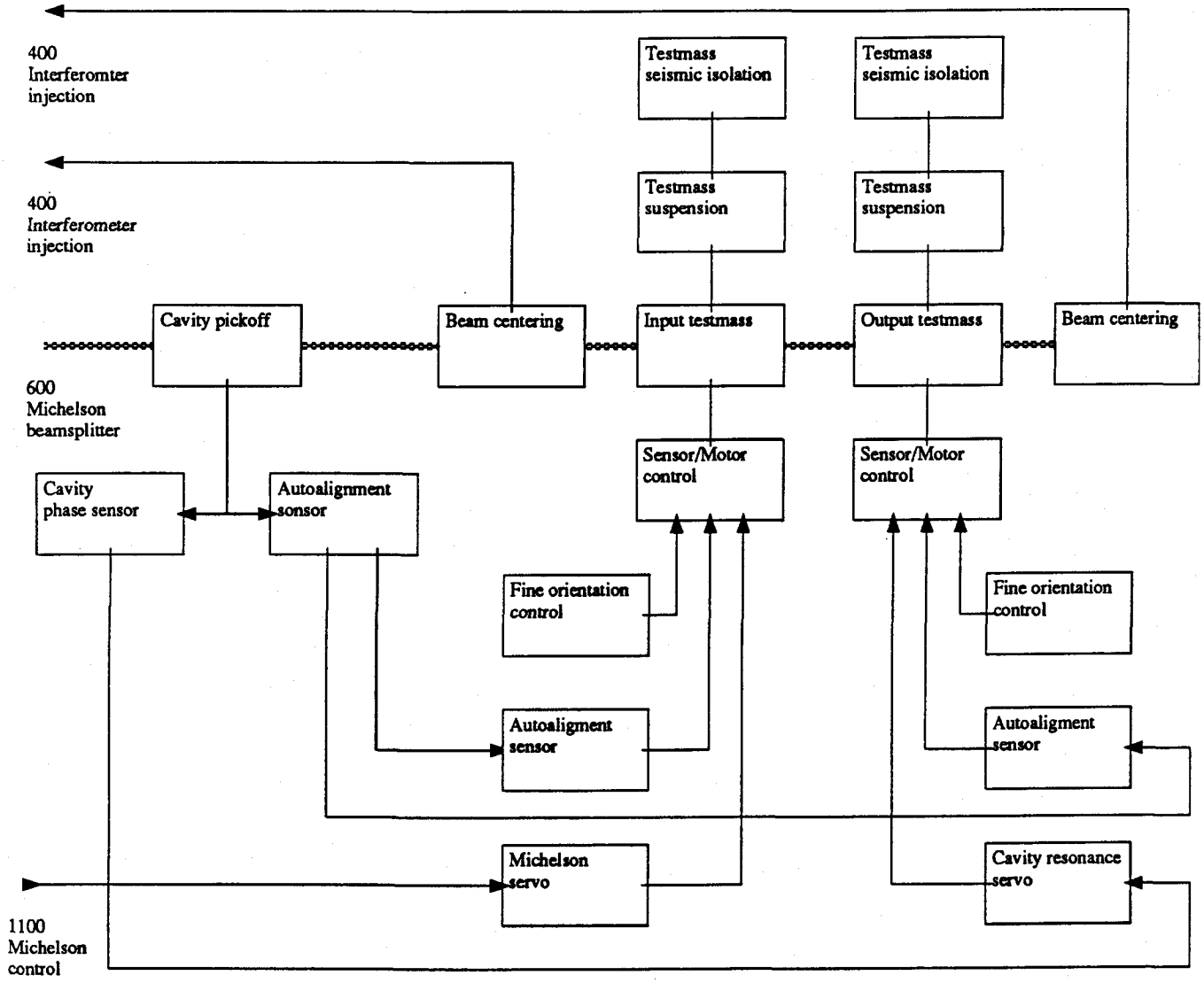

Figure 2.10: Block diagram of interferometer subsystem ICD800, the Right Cavity of the main interferometer.

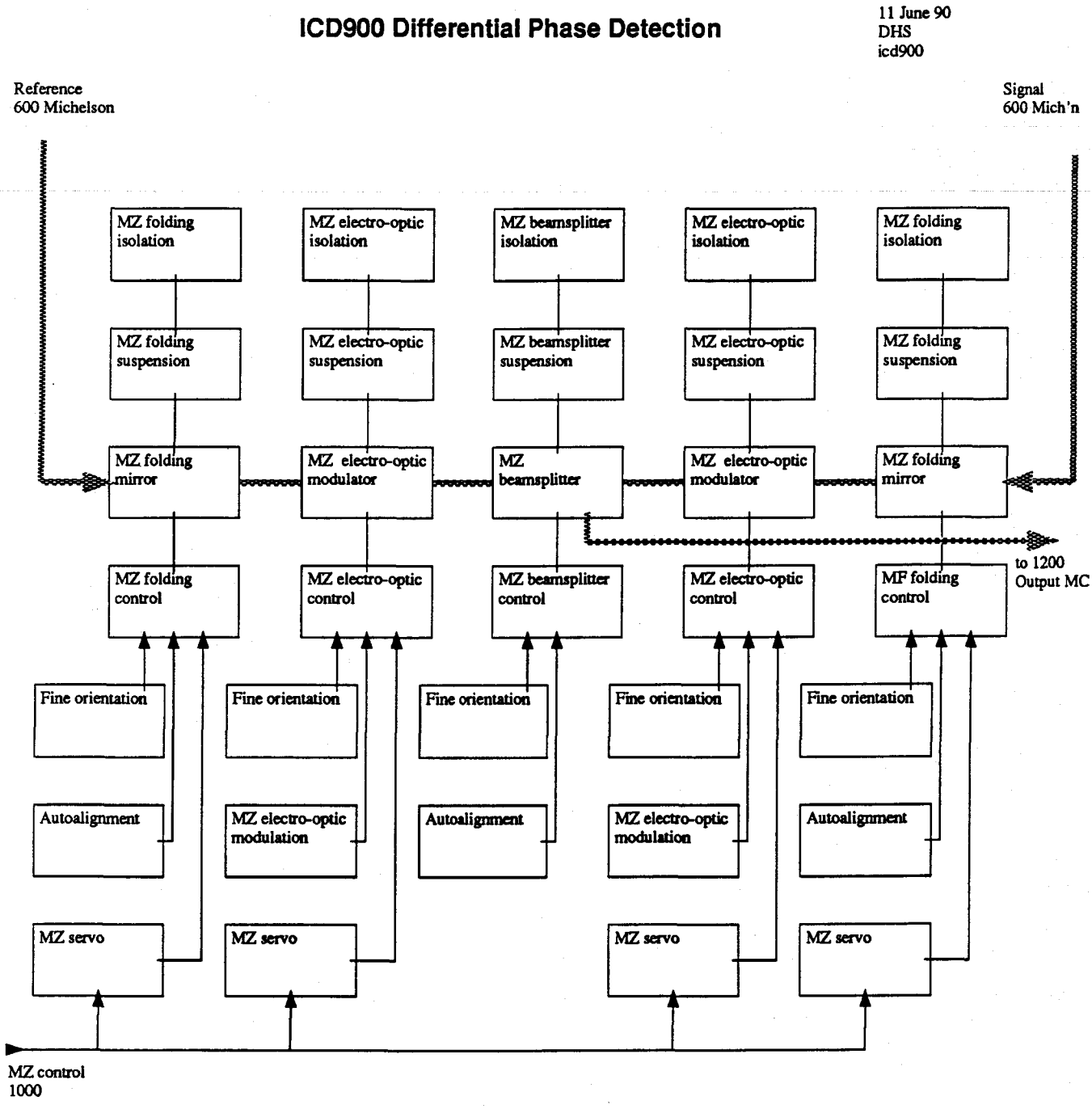

Figure 2.11: Block diagram of interferometer subsystem ICD900, the Differential Phase Detection system.

TBD

Figure 2.12: Block diagram of interferometer subsystem ICD1000, the Differential Phase Detection Control sytem.

TBD

Figure 2.13: Block diagram of interferometer subsystem ICD1100, Michelson Control system.

TBD

Figure 2.14: Block diagram of interferometer subsystem ICD1200, the Output Mode Cleaner system.

TBD

Figure 2.15: Block diagram of interferometer subsystem ICD1300, Strain Readout system.

Chapter 3

Common Component Classifications

file compclass.tex, 10/11/90

The figures and text of Section 2.2 show many repeated functional blocks and subsystems. Most design problems or uncertainties are not specific to a given subsystem, but appear in several different contexts. In these cases it is desirable to define a relatively compact class of components of a given type and research the common features of the class together. In many instances this research may lead to a single "universal" design which can fill a slot anywhere in the interferometer. In other cases, attacking the problem generically may reveal that there is an assortment or hierarchy of solutions, suited to various applications.

Major common component categories already apparent are outlined below; headings represent various classes of elements, and the subheadings give examples of members of each class. This outline will be replaced by technical documentation as the design process continues, and it is hoped that eventually it will be possible for the design team to view this chapter as a resource for basic interferometer building blocks.

Existing design study information and the results of LIGO working papers will also be included as appropriate.

1. Mirrors
   - (a) test mass
   - (b) recycling
   - (c) beamsplitters
   - (d) beam samplers

(e) folding mirrors

2. Lenses

   (a) fiber coupling
   (b) gaussian beam matching
   (c) expansion telescope

3. Isolation and Suspension Systems

   (a) test mass
   (b) beamsplitter/folding mirror
   (c) injection/output optics
   (d) auxiliary cavities

4. Local Control Sensors and Drivers

   (a) test mass
   (b) beamsplitter/folding mirror
   (c) injection/output optics

5. Beam/Optic Orientation

   (a) mechanical
   (b) local reference
   (c) global reference

6. Automated Alignment

   (a) cavity
   (b) recombined beam interferometer

7. Modulation and signal recovery

   (a) cavity in reflection
   (b) cavity in transmission/coupled cavity
   (c) interferometer

8. Servo Control Systems
   (a) laser stabilization
   (b) cavity locking techniques
9. Data and Control System Interfaces
   (a) monitor/set points
   (b) control loops
   (c) data archiving
   (d) test input/output

Chapter 4

Interferometer Data and Control System

file dcschapt.tex, 10/10/90

The data and control system will play an integral role in the functioning of the interferometer. One clear role is to allow strain data to be archived and evaluated, along with ancillary information which makes the data useful: time stamps, housekeeping data, and so forth. It will also allow on–line analysis of the data, and trigger storage of time buffers of detailed interferometer status data.

The data and control system (henceforth DCS) will also be used to monitor and control interferometer operations. Housekeeping data will be displayed graphically, errors flagged, and trends recorded. Sequencing of locking and alignment will be controlled, as will be set points of various parameters. Interlocks will prevent damage to interferometer systems. Control loops of various bandwidths may have partly or totally digital implementations. Controlling and monitoring distant end– and mid– stations is also part of the DCS mission.

Finally, a very important role will be to allow troubleshooting of interferometer system functions. Wide bandwidth measurements of transfer functions, correlations, and online modelling (roles now played by standalone signal analyzers in prototype research) should be possible through or in concert with the DCS. The ability to make these measurements in a transparent, flexible way is imperative to attaining full operation in the minimum time.

The design of the DCS both influences and depends upon the design of the interferometer. Although it is early in the interferometer design process, some

outline of the DCS is already visible, and much of the overall architecture can be foreseen. The following descriptions reflect our current knowledge of the DCS requirements and the available techniques for achieving them; both will be revised substantially. In particular, numerical values have been chosen only to get the definition process started, and should not be construed as specifications.

4.1 Data Types and Bandwidths

Exactly which signals are to be exchanged is best developed in conjunction with the design of each subsystem, where information flows are explicitly indicated. As the design advances, these lists of signals with their associated bandwidths, precision, duty cycle, and other relevant information should be collected in this section. To limit the complexity of the hardware and software, it is worthwhile to try to limit the number of different kinds of interfaces. We will use the name 'unit' here to mean one sub-sub-system, capable of generating and receiving signals; it would typically be one or a few NIM or VXE modules, the kind of boxes which were shown, for example, in Figure 2.3.

4.1.1 Bandwidths

We propose standardizing to (approximately) four bandwidths in the system. These are low-bandwidth (henceforth LB), which is of the order of 10 Hz; medium bandwidth (MB), of the order of 1 kHz; wide bandwidth (WB), of the order of 10 kHz; and very wide bandwidth (VWB), of the order of 100 kHz. A word sampling rate of 2.5 times the bandwidth is proposed. Data is for now assumed to be carried in 16-bit words. Often several bits will be unused, but there may arise instances where two words (32 bits) are required to preserve dynamic range for certain critical signals.

4.1.2 Mode and Status

This is LB digital information sent or received. Received from the DCS are typically commands for on/off, gain high/medium/low, send out monitor data from test point 1,2,3... etc. Sent to the DCS are acknowlegements,

in/out of lock, in/out of range, error, etc. One 16-bit register should be sufficient for a given 'unit'.

4.1.3 Housekeeping

This is LB analog information, encoded by a unit or by a crate serving several units. Typical signals are temperatures, mechanical drifts, and vacuum system pressures or partials.

4.1.4 Set Points

This is LB analog or digital information, sent to a unit to define certain reference values or operating targets. Typical signals are coarse motor control instructions, high voltage offsets, RF drive levels, and laser power.

4.1.5 Monitoring

This is MB analog information, encoded by a unit or by a crate serving several units. Seismic monitors, magnetic and RF field monitors, line power, and so forth are in this category.

4.1.6 Suspension, Alignment Signals

This is MB analog information, encoded by a unit or by a crate carrying the unit.

4.1.7 Servo Error, Control Signals

This is WB analog information, encoded by a unit or crate.

4.1.8 Test Inputs/Outputs

This is VWB information sent to or received from a unit. It is used for diagnostics and special tests, not for normal monitoring or archiving. It allows many research measurements to be made without connecting an external test apparatus to a specific unit. It is possible to share a limited number of test

input/output channels among the units in a given crate or system, since most tests will not involve all units simultaneously.

4.2 System Hardware Architecture

The overall system architecture will be like that described in the LIGO construction proposal (reference [2], volume 2, page 68 and following pages). In this example, the backbone of the communication system is an Ethernet, running a standard protocall such as TPC/IP; workstations, slow environmental monitoring, and the like are directly connected. The interferometer monitor, control, test, and archiving data must have a predictable latency, and should probably be on a separate bus; however, the physical dimensions of the interferometer DCS will probably not allow direct use of VME bus architecture or its equivalents throughout. Limiting those signal paths with critical timing requirements to relatively small local subnets will relieve the above constraint somewhat. The remote (end– and mid–) stations will probably be connected via optical fiber to the apex building, and this will require some kind of bus translation. Some relatively basic topics concerning strategy and format are further discussed below.

4.2.1 A/D and D/A Conversion Interface Level

For most applications a relatively clean solution would be to put the converters directly in each interfaced unit. This may grow costly for WB and VWB applications, so it is likely that some mixture of centralized conversion with analog signal transmission (and switching) and distributed conversion with digital transmission will result. It is unlikely that costs will push this centralization beyond the scope of crates, bins, or racks, so the proliferation of analog signal wires traversing the facility can probably still be avoided.

4.2.2 Local Digital Control Loops

Clear candidates are suspended mass damping, orientation systems, automated alignment, slow drift correction servos, and fringe acquisition. A significant difficulty may remain in that the dynamic ranges of many existing

prototype subsystems would imply conversions of over 20 bits resolution, with corresponding linearity, to reach equivalent performance.

4.2.3 Special-purpose Computing Equipment

Low-level autoaligment processing will aid in obtaining understandable, orthogonal error signals. Pattern recognition systems may be used to find beams, and DSP units which do efficient Fast Fourier Transforms are also strong possibilities.

4.2.4 VWB Input/Output Selection, Processing

The widest bandwidth signals will have a low duty cycle. Typically, two or three of these signal outputs would be recorded for a limited time while a predetermined signal (noise or other excitation) would be applied to a test input. It will be important to determine how many simultaneous test channels need to be available at any given time, and how long tests need to last, since this will tend to drive the total system data transmission rate.

4.2.5 Maximum Response Time

This is a trade-off with the amount of local processing. The various subsystems must make sure that no problems would occur if their demand for attention were not acted upon within a certain time.

4.3 System Software Architecture

Some vague generalities about the software follow.

4.3.1 Operating Systems

The operating system for the workstations and most of the computers on the Ethernet backbone should be Unix. As little low-level programming as possible should be done. The laboratory experience with RTU (Concurrent) will help determine what role this operating system should play. VxWorks (Wind River Systems), and/or other low-level operating systems should be used where speed and response latency are important.

4.3.2 Data Access

Users on the Ethernet backbone should be able to get access to FIFO buffers where the various signals will be stored. Graphical display of these data, vs. time, frequency, other variables, should be possible. A "user–friendly" environment is crucial, since many scientists and engineers will need to gain access throughout the R&D and observation modes.

4.3.3 Monitor

A status screen (or screens) showing the status of the entire interferometer is needed. Flagging of abnormal conditions, and graphical displays of the evolution of housekeeping variables are needed.

4.3.4 Troubleshooting

Much of the initial work with the interferometer will be to troubleshoot and understand the new system. A means of looking at different signals, with large bandwidths (VWB) well in excess of the highest astrophysical signals is needed; and the ability to inject test signals (noise, swept sine, etc.) would be desirable.

Chapter 5

Commissioning and Testing

5.1 Subsystem and Assembly Tests: Campus or Vendor Site

TBD

5.2 Interferometer System Tests and Commissioning: Observatory Site

file intsystest.tex, 10/12/90

It will be invaluable to bring each interferometer on–line in a series of graduated steps to ensure that its systems are performing as intended. Because this commissioning procedure will influence the design (some subsystems must be made to operate in a 'stand-alone' fashion, and some interconnections must be made in a flexible way), a commissioning procedure should be adopted

early in the design process. A proposed procedure is given below, where the subheadings describe tests and information to be obtained.

1. Michelson, short (to near mirrors)
   (a) pointing of near mirrors
   (b) figure of beamsplitter, near mirrors, ext. det. optics
   (c) locking
   (d) external detection
2. Michelson, long (to far mirrors)
   (a) rough matching to far mirrors
   (b) pointing of far mirrors
   (c) figure of far mirrors
   (d) scattering
   (e) symmetry (length)
   (f) servo with 4 km delay
3. recycling with Michelson (short, long?)
   (a) rough matching
   (b) reasonable sensitivity (mirror motions ok?)
4. one 4 km arm cavity (no beamsplitter)
   (a) matching
   (b) locking of cavity
   (c) (auto)alignment of cavity
   (d) measurement of frequency noise
5. recycling mirror with one arm
   (a) matching
   (b) locking

(c) loss

6. other arm alone

   (a) BS pointing

   (b) similarity of matching to above

7. full recombination

Appendix A

Handbook Distribution and Update Information

file distrib.tex, 10/6/90 MEZ

This handbook is intended to be a working document, whose authorship includes in varying capacities the entire LIGO team. To provide free access to the information contained while avoiding a confusing proliferation of document versions, we request reasonable adherence to the following rules:

- A **Handbook Organizer** will be appointed to keep track of updated handbook information and keep a current **Master Handbook**. *As of 10/6/90, M. Zucker has volunteered to take the first shift as Handbook Organizer.*
- Complete, edited contributions to the Handbook should be submitted to the Handbook Organizer for inclusion, after suitable approval by the Interferometer Conceptual Design team.
- Master Handbook computer files will be kept in a group–readable, owner–only–writable subdirectory of the current Handbook Organizer's account[1]. The Organizer is responsible for ensuring that only the Master is printed or copied for distribution; it is thus necessary for all

[1]It may also be useful to keep an updated Master file set on the filesystem of the other LIGO campus site, in case of communication difficulty; the Organizer should designate the location of these files and see to their maintenance, with assistance from a representative of the other group.

submissions and revisions to be added to the Master files by the Organizer. *As of 10/6/90, M. Zucker is keeping the master file set in the directory* `mike/iicd/handbook/master` *on the machine* `ligo`.

- Only three (3) additional paper copies of the handbook shall be automatically updated to the latest revision date; one of these **Secondary Master** books will reside in the MIT Science Team Library, one in the Caltech Science Team Library, and one in the Engineering Library. All other copies will be labelled **Uncontrolled Copy**, and should not be duplicated or distributed. It will be the responsibility of each owner of an Uncontrolled Copy to update or destroy it as it becomes obsolete.

- Current, updated Uncontrolled Copies of the Master will be available upon (reasonable) request from the Organizer; the Organizer will help the administrative staff to assemble these when needed, and will also supervise the updating of the Secondary Master handbooks. Use of the library Secondary Masters and the computer files is encouraged to avoid wasteful duplication.

Appendix B

Campus Research Related to Conceptual Design

file campres.tex, 10/12/90

B.1 Research and Development Strategy

We expect the completion of the conceptual design for LIGO interferometers to proceed by stages, roughly outlined below. At this writing (October '90) we have made progress in the first three phases; further progress will involve some prioritization and assignment of research tasks to the overall LIGO team, addressing those open topics discussed in Sections B.2 and B.3 below.

1. top-level functional breakdown of the interferometer
2. second-level functional breakdown showing repeated elements of the design
3. description and specification of the second-level breakdown systems
4. identification of critical research areas
5. time-lines showing the ordering of research efforts to resolve questions
6. research to determine specifications and design details
7. third-level functional breakdown showing detailed design
8. breakdown in engineering disciplines

The research and development on the campuses should proceed in parallel with the design effort. An example "flowchart" showing how design, engineering and campus R&D might work together to produce final specifications for interferometer subsytems (Section 2.2) or common component classes (Chapter ??) is presented in Figure B.1.

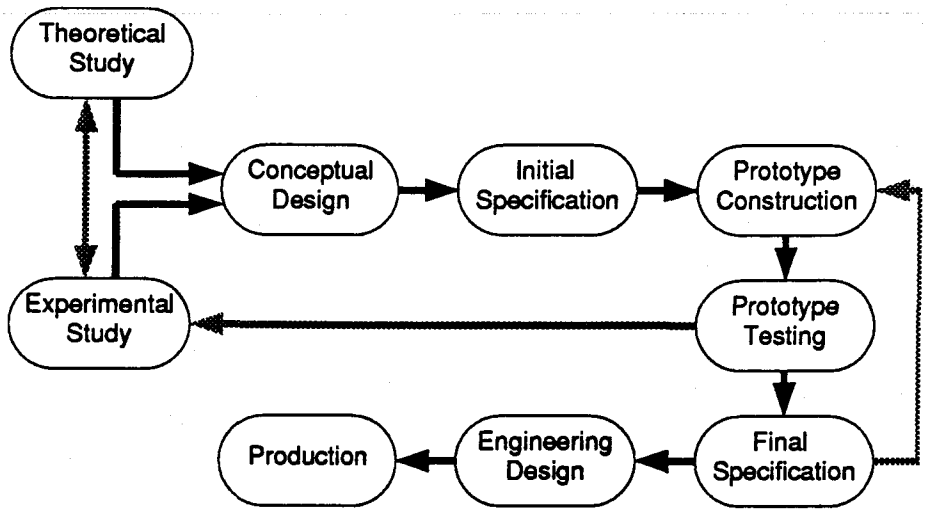

Figure B.1: Generic procedure for developing interferometer subsystems, components and techniques.

B.2 Research Activities Motivated by Conceptual Design Issues

A list of research projects that must be performed to arrive at a working design comes as a natural outgrowth of the initial conceptual design exer-

cises. This list is summarized below. Many of these projects are already underway; those that are not are shown in boldface. Following the summary, in Section B.3, is a more detailed breakdown of those projects which are not now (September '90) actively underway.

1. OPTICS
   (a) **Spatial and temporal mode cleaners, input and output (fibers/FPs)**
   (b) Optical power handling capability
   (c) HR, BS, and AR coating improvements/characterization
   (d) Electro-optic modulators for LIGO: specifications, design, and test
   (e) Optical Isolators for LIGO: specifications, design, and test
   (f) Numerical optics (mostly GLADV)
   (g) Recycling, Modulation, Signal Recovery techniques
2. ISOLATION/SUSPENSION
   (a) **Component suspension and local control/damping**
   (b) Thermal noise research: calculations and lab. measurements
   (c) Component isolation (stacks)
3. CONTROL SYSTEMS
   (a) **Beam alignment and orientation systems**
   (b) **Servo systems modelling and design**
   (c) Automation of interferometer control and monitor
   (d) Calibration system for LIGO
   (e) (Data and control system)
4. INTERFEROMETRY
   (a) Current 40m prototype investigations
   (b) Rigid interferometer investigations
   (c) General hanging interferometer tasks, 5 and 40 m prototypes

(d) 5 Meter Suspended Prototype Design/Construction

(e) 40 Meter Prototype Reconfiguration/Reconstruction

5. TRANSFER TO ENGINEERING

(a) **Laser and pre-stabilization**

B.3 Critical New Tasks

The topics and/or tasks listed in this section have been identified by the Interferometer Conceptual Design team as having a crucial impact on subsequent stages of the design, and are not yet under active investigation.

As of September 1990

1. Spatial and temporal mode cleaners, input and output (fibers/FPs):

(a) calcs. for needed suppression of position and freq./ampl. noise

(b) propose/predict performance/build prototype system(s)

(c) non-interferometer (ifo) tests of effectiveness

(d) tests at input and output of prototype ifo

(e) design for LIGO mode cleaning subsystem

2. Component suspension and local control/damping:

(a) establish hierarchy for different component classes:

(b) sensors: S/N needed, side effects (e.g., vanes on masses)

(c) controllers: force needed, side effects (e.g., Q)

(d) evaluation of existing systems

(e) input from calcs of servo forces and dynamic range needed

(f) expts. on suspension techniques (e.g., influence on Q)

(g) input from thermal noise calculations and measurements

(h) relationship to isolation system

(i) lab. construction and test

(j) hanging ifo tests

(k) design for LIGO component suspension and damping

3. Beam alignment and orientation systems:
   (a) establish initial constraints: bandwidth, precision
   (b) choice of sensing method (RF, dithering); simple or hierarchical
   (c) lab bench tests
   (d) hanging ifo tests
   (e) design for LIGO alignment system
4. Servo system modelling and design:
   (a) global analysis and breakdown of servos
   (b) spectra of input disturbances (seismic, frequency)
   (c) allowable deviations from null point (spectral, peak)
   (d) servo bandwidth needed, possible (given delays)
   (e) locking schemes for cavities
   (f) hanging ifo tests
   (g) design for LIGO main cavity servos
5. Transfer to engineering of laser stabilization

Appendix C

40m Prototype Configuration

TBD

Appendix D

5m Prototype Configuration

TBD

Bibliography

file references.tex, 10/8/90

[1] Rochus E. Vogt, Ronald W.P. Drever, Kip S. Thorne, and Rainer Weiss, *Caltech/MIT Project for a Laser Interferometer Gravitational Wave Observatory,* Renewal Proposal to the National Science Foundation. California Institute of Technology and Massachusetts Institute of Technology (1987).

[2] Rochus E. Vogt, Ronald W.P. Drever, Kip S. Thorne, Frederick J. Raab, and Rainer Weiss, *The Construction, Operation, and Supporting Research and Development of a Laser Interferometer Gravitational-Wave Observatory,* Proposal to the National Science Foundation. California Institute of Technology (1989).

[3] Stanley E. Whitcomb, "Shot Noise in the Caltech Gravitational Wave Detector—The Mid-1984 Configuration," unpublished research communication. California Institute of Technology (1984).

[4] Carlton M. Caves, "Quantum-Mechanical Radiation-Pressure Fluctuations in an Interferometer," *Phys. Rev. Lett.* **45** (2), p. 75 (1980).

[5] S.E. Whitcomb, "Optical Pathlength Fluctuations in an Interferometer due to Residual Gas," unpublished communication (1984).

[6] D. Shoemaker, R. Schilling, L. Schnupp, W. Winkler, K. Maischberger, and A. Rüdiger, "Noise behavior of the Garching 30 meter prototype gravitational wave detector," Max-Planck-Institut für Quantenoptik manuscript MPQ 130 (1987).

[7] A.A. Michelson and E.W. Morley, "On the Relative Motion of the Earth and the Luminiferous Ether," *American Journal of Science* **XXXIV** (203), p. 333 (1887).

[8] A. Rüdiger, R. Schilling, L. Schnupp, W. Winkler, H. Billing and K. Maischberger, "A mode selector to suppress fluctuations in laser beam geometry," *Optica Acta* **28** 5, p. 641 (1981).